Lisa Theresa Langmann, BSc.

Photoacoustic Spectroscopy for non-invasive determination of lactate concentration

Master's Thesis

to achieve the university degree of

Diplom-Ingenieurin

Master's degree programm Biomedical Engineering

Submitted to

Graz University of Technology

Supervisor

Univ.-Prof. Dipl.-Ing. Dr.techn. Christian Baumgartner

Institut für Health Care Engineering mit Europaprüfstelle für Medizinprodukte

Univ.-Prof. Mag.rer.nat. Dr.rer.nat. Alexander Bergmann

Graz, August 2018

Eidesstaatliche Erklärung
Affidavit

Ich erkläre an Eides statt, dass ich die vorliegende Arbeit selbstständig verfasst, andere als die angegebenen Quellen/Hilfsmittel nicht benutzt, und die den benutzten Quellen wörtlich und inhaltlich entnommenen Stellen als solche kenntlich gemacht habe. Das in TUGRAZonline hochgeladene Textdokument ist mit der vorliegenden Masterarbeit identisch.

I declare that I have authored this thesis independently, that I have not used other than the declared sources/resources, and that I have explicitly indicated all material which has been quoted either literally or by content from the sources used. The text document uploaded to TUGRAZonline is identical to the present master's thesis.

Datum *Date*	Unterschrift *Signature*

Acknowledgements

First, I want to thank my parents and my brother, who helped me throughout my years of study, through the process of researching and writing this thesis and gave me emotional support.
Further I want to thank my two supervisors Univ.-Prof. Dipl.-Ing. Dr.techn. Christian Baumgartner and Univ.-Prof. Mag.rer.nat. Dr.rer.nat. Alexander Bergmann. In particular Univ.-Prof. Mag.rer.nat. Dr.rer.nat. Alexander Bergmann supported me with his expert knowledge and always helped me to find the right answers to my scientific problems.
Finally, I want to thank all my friends who always helped me and made the academic studies an unique and extraordinary experience.

Table of Contents

List of Figures

1 Abstract

Titel
Photoakustische Spektroskopie für die nichtinvasive Bestimmung der Laktatkonzentration

Zusammenfassung
In der Medizin ist es von großer Bedeutung so viele nichtinvasive Tests wie möglich anbieten zu können, um Schmerzen zu minimieren, Personalkosten einzusparen und Krankheiten frühzeitig zu erkennen. Aus diesem Grund wurde im Rahmen dieser Masterarbeit eine Machbarkeitsstudie zur Messung des Laktatwertes im Blut durchgeführt. Dieses Laktat und drei weitere biologische Moleküle: Harnstoff, Glukose und Cholesterin, wurden mittels Simulation, Spektrometrie und Photoakustischer Spektroskopie bestimmt. Ziel ist es, eine Machbarkeitsstudie durchzuführen, bei der ein Sensor entwickelt wird, der auf photoakustischer Spektroskopie basiert. Ein mögliches Einsatzgebiet dieses Sensors liegt im Fitnessbereich

5 Schlüsselwörter
Laktat, Photoakustische Spektroskopie, Blutkonzentration, Simulation und Schaltungsdesign

Title
Photoacoustic Spectroscopy for non-invasive determination of lactate concentration

Abstract
In medicine it is important to conduct as many tests as possible non-invasively in order to obtain reduction in pain, minimize staff costs and diagnose diseases in an early stage. This master thesis examines the possibility of measuring blood lactate concentrations non-invasively. Urea, glucose and cholesterol have also been investigated to avoid signal overlap issues. Those different biological molecules were examined with simulation, spectrometry and photoacoustic spectroscopy. The target is a feasibility study to create a sensor, which is based on photoacoustic spectroscopy and can be used for instance in fitness applications.

5 Key words
Lactate, Photoacoustic Spectroscopy, blood concentration, simulation and printed circuit board design

2 Introduction

The aim of this master thesis is to measure lactate non-invasively with the use of light. In medicine, it is an aspiration to have as many non-invasive tests as possible. The advantage of non-invasive measurements is that the patient does not get hurt and often no medical professional is needed, overall lowering staff costs. In the future a lactate sensor could be constructed based on the findings of this work. This sensor would be used as a basic device in the fitness segment and therefore allow athletes to measure their lactate values themselves. Currently only invasive blood lactate measurement is possible.

This test has the patient working out on an ergometer for a specific timeframe with a nurse or a doctor taking blood samples from the earlobe at particular intervals. A comparison between baseline values and the acquired stress blood samples determine the results of the test. With this method a medical professional is necessary and it cannot be conducted at home. The motivation for this master thesis was to solve this problem and enable a non-invasive solution.

The method chosen, was to use light to stimulate the lactate in the blood, but none of the other biological molecules. Lactate shows absorption in the infrared region of the electromagnetic spectrum. The ubiquity of approved medical devices using infrared light shows this to be a good approach. For this thesis photoacoustic spectroscopy was used to determine lactate concentrations. This type of measuring technique is very common for quantifying aerosol and gas concentrations, but there are also several studies, especially for glucose measuring, which used this method in liquids [1]. A benefit of this physical measuring method is that it is non-invasive, cheap and with further research it could be portable. To investigate if it is possible to measure solely lactate. Other molecules with large chemical likelihood to interfere, have been also researched. Urea, glucose and cholesterol have been identified. In addition, a simulation and a spectrometry experiment to approach the photoacoustic measurement was conducted. Within this simulation the aim was to find the perfect filter to measure lactate concentration in the presence of other molecules. To this end, complete spectra were obtained of the four biological molecules.

To summarize, in the future there will be more medical non-invasive tests to save time and money. With this thesis, we tried to develop a non-invasive lactate measurement method, for future implementation.

3 Task

For this thesis with the title "Photoacoustic spectroscopy for the non-invasive determination of the lactate concentration" a literature research has to be conducted to understand the lactate characteristics. The remaining master thesis is divided into three different areas of work. First, the lactate peaks at 2247 nm and 2299 nm were determined by a MATLAB simulation. For a precise integration of those peaks, two diverse filtering methods have been used: an Etalon and a combination bandpass, which consists of two bandpasses. With these methods it should be able to only determine the lactate peaks in presence of other biological molecules. In the end, a comparison between those two filters should be done and the best fit should be selected.

Secondly, spectrometry measurements should be carried out. Within this technique, the four biological molecules lactate, urea, glucose and cholesterol should be measured directly in powder form. Afterwards a measurement of the biological molecules in blood concentrations should be performed. It should be verified if the minute concentrations dissolved in distilled water can be determined. For this task, a special setup is needed and 3D-printing would be necessary to guarantee repeatability and reproducibility.

Finally, to identify the lactate peaks a photoacoustic spectroscopy should be performed. Within this measuring method, it is essential to design a printed circuit board (PCB), which is able to determine the very weak photoacoustic signal of lactate. The microphone should be carefully chosen so that it is able to measure in liquids. To obtain a stronger signal of the weak alternating signal without any background noise, a digital Lock-in amplifier should be used. 3D-printing is again needed to have repeatable and a reproducible measurements.

4 Basic principles in measuring lactate concentrations

4.1 Light – Wavelengths of radiation

In this chapter a short introduction into optical radiation and light is given. Light has characteristics and properties of both a particle and a wave. The energy momentum like a particle and the wavelength and frequency like a wave. Therefore is light a unique particle (photon) with zero mass. [2] Optical radiation are all electromagnetic waves and fields with a photon energy less than 12.4 eV and the wavelength has to be between 100 nm and 1 mm [3]. With higher wavelength, the photon energy is decreasing. In contrast, the depth of penetration is increasing. The behaviour of electromagnetic radiation depends on its wavelength. Higher frequencies have shorter wavelengths and vice versa. **Figure 1** shows the optical radiation categorized into three different areas.

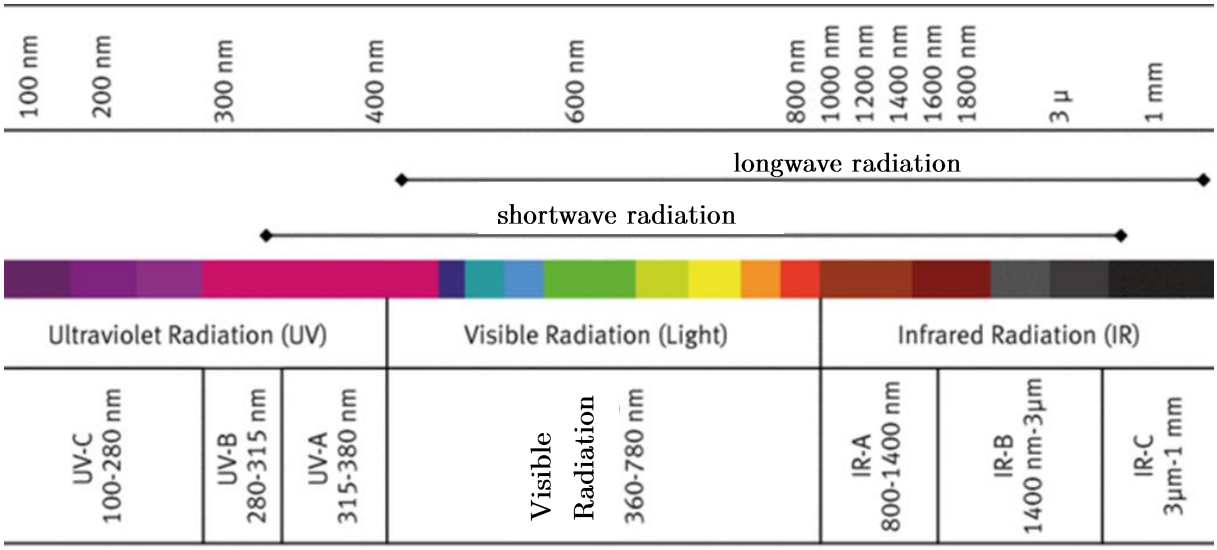

Figure 1 Wavelength range of electromagnetic radiation [4]

At short wavelengths, you have the ultraviolet radiation (UV). Approximately 7% of the total light output of the sun is UV radiation [5].The UV-band is in between of the X-ray band and the visible region. With the high amount of energy of the short wavelength UV radiation it is possible to break chemical bonds and carry out photochemical reactions [6]. Over decades, many papers show human health-related effects by absorbing ultraviolet radiation through the skin. Obviously, UV radiation can carry many risks, but potentially also many benefits for the human health. The number one risk is a sunburn because of sun

exposure. This can lead to skin damage and even to cancer. Particularly the UV-B and the UV-A band cause health problems. For this reason, the human population are using sun cream to avoid these risks. On the contrary, UV-C radiation gets absorbed by the atmosphere and therefore is not problematic harmful for humanity. Yet, there are still positive effects from the UV radiation to the human body. For instance, it is essential for the production of vitamin-D. Without vitamin-D people cannot survive [3]. However, the harmful effects outweigh the benefits. UV light is invisible to the human eye, because it is absorbed below at 360 nm by the cornea as well as below 400 nm by the internal lens.

Second part of the graphic shows the visible radiation. The visible spectrum is the portion of optical radiation visible to the human eye, which responds to wavelengths from 400 to 700 nm. Some individuals can perceive wavelengths from 380 to 780 nm [6]. Nearly 39% of the solar radiation that reaches the earth is of the visible light region [6]. Violet is the shade with the highest photon energy, the weakest photon energy, can be measured in red light. In the 17th century Isaac Newton discovered that white light can be divided with a prism into the spectral colours. Visible light does not have such harmful effect on human skin, because the percentage of the reflected light compared to the UV radiation is much higher with 45% to 60% [3]. Also it is low-energy in contrast to the UV light. Visible light can also induce indirect DNA damage by generation of ROS (reactive oxygen species) [6]. Cell aging is another drawback of absorbing too much light. Fortunately, visible light is used for treatment of many dermatosis and for cosmetic purposes, through its use in phototherapy devices such as IPL (intense pulsed light technology), lasers and in PDT (photodynamic therapy) [6].

The third and last part of the graphic captures the infrared region. For my thesis, this is the most important area, because all the measurements are taken within this wavelength range. Infrared radiation constitutes the waveband longer than 780 nm and up to 1 mm. It accounts for approximately 40% of the solar radiation reaching the ground at sea level [5]. **Figure 2** shows the infrared radiation, which can also be divided into three bands. The first one includes the 800 to 1400 nm range and is called IR-A region. The band between 1400 to 3000 nm is called IR-B. IR-C is between 3000 nm to 1 mm. The infrared radiation is able to

penetrate the skin layers: epidermis, dermis and subcutaneous tissue to differing extents, depending on the exact wavelength as shown in **Figure 2**.

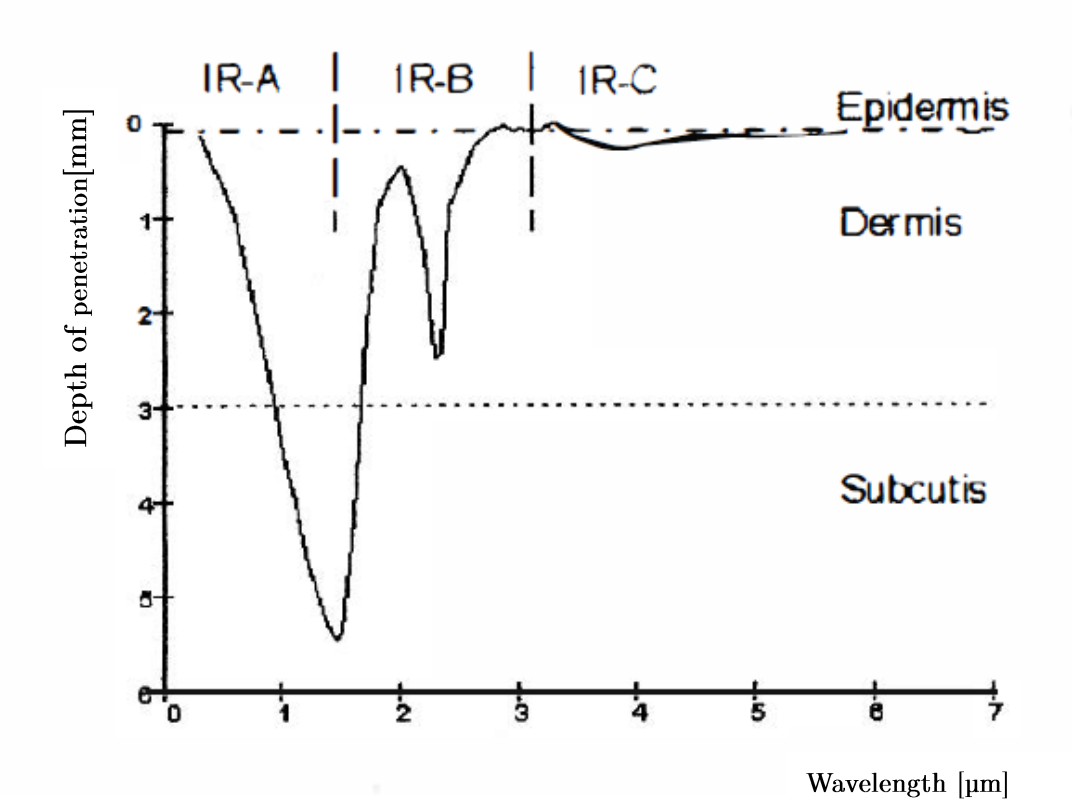

Figure 2 Different penetration depth depending on the IR band [3]

The IR-B region is the most significant for photoacoustic lactate measurement, because all the relevant peaks of lactate, urea, cholesterol and glucose are within this 1400 nm and 3000 nm band. IR exposure is perceived as heat [7]. This heating effect is especially often used as therapy in dermatology. The most common application effect is used in laser technology. For this technique the essential chromophore is water. By laser application the tissue water is heated up quickly, leading to overheating and therefore coagulation, allowing for incision [3]. However, chronic IR exposure can be harmful to the skin. First sightings of those effects were on the legs of people sitting to close to open fire. Those leaded to erythematous or to hyperpigmented dermatoses. Nowadays, there are laptop-computer induced erythemas possible. Although, those side effects outweigh the possibility to heal cutaneous malignancies [5]. IR applications in medicine are in the normal use not harmful only after longterm application. The NIR percentage from solar radiation however cannot harm a human, because of the low concentration of the sunlight. Infrared radiation is mostly

harmless, because of the low photon energy. In the table below the adverse biological impact of light onto skin is shown.

The most beneficial effects which are often used in medical devices need a lot of electrical power. The higher the power gets the more effect can be recognized onto the body.

Table 1 Biological response of light in the different regions [8]

Light region	**Penetration depth into skin with resulting damage**	
UV-C, UV-B (100 – 315 nm)	<< mm	Redness, skin aging, carcinomas
UV-A (315 – 400 nm)	~ 1 mm	Heavy pigmentation
visible (400 – 780 nm)	Depending on pigmentation	Photochemical/thermal damage
IR-A (780 – 1400 nm)	Depending on pigmentation	Thermal damage
IR-B (1.4 – 3 µm)	~ 1 mm	Thermal damage
IR-C (3 µm – 1 mm)	<< mm	Thermal damage

4.2 Lactate Characteristics

Lactate is the anion of lactic acid. It is the conjugate base of the lactic acid. This anion is commercially available with a variety of counter ions. It exists in 2 optical isomeric forms, L-lactate and D-lactate. Only the right-handed L-lactate form is produced in human body and therefore is commonly measured, it is shown in **Figure 3**. The left-handed D-lactate is a byproduct of bacterial metabolism and only appears in humans with gut illnesses like short bowel syndrome [9].

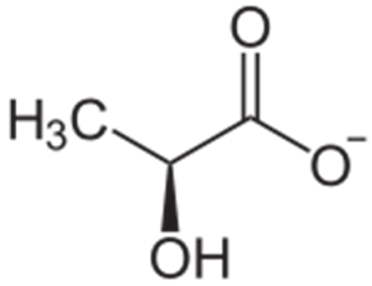

Figure 3 chemical structure of L-Lactate [10]

The chemical structure formula of lactate is $C_3H_5O_3^-$. Blood lactate concentration is a parameter of the anaerobic metabolism. If there is not enough oxygen to support the normal energy production, which is aerobic, lactate gets produced [11]. Hence, it is traditionally used to monitor tissue oxygenation. Lactate is one of the most commonly measured parameters during exercise testing for medical or for competitive sports purposes. With the blood lactate value it is possible to evaluate the underlying pathology, because lactate values elevate before abnormalities can be seen in heart rate, blood pressure or urine output [12].

Lactate concentrations in the human body depend mainly on the measuring location. For this study, the focus was set on the blood lactate concentration with values of 5-20 mg/dl or 0.55–2.2 mmol/l. In comparison, the normal lactate concentrations are 11–19 mg/dl in the liquor and 9–16 mg/dl in the synovial fluid [10]. During exercise the lactate values temporarily increase to up to 20 mmol/l due to momentary oxygen debt in muscle cells [13].

4.2.1 Lactate Metabolism

Lactate is a by-product of the glucose metabolism, which is the main adenosine triphosphate (ATP)-producing process. During this process, glucose transforms to pyruvate, which then can follow two different pathways: anaerobic glycolysis with lactate as end product and aerobic glycolysis, which includes the citric acid cycle (Krebs cycle) and the oxidative phosphorylation. **Figure 4** illustrates the previous mentioned steps.

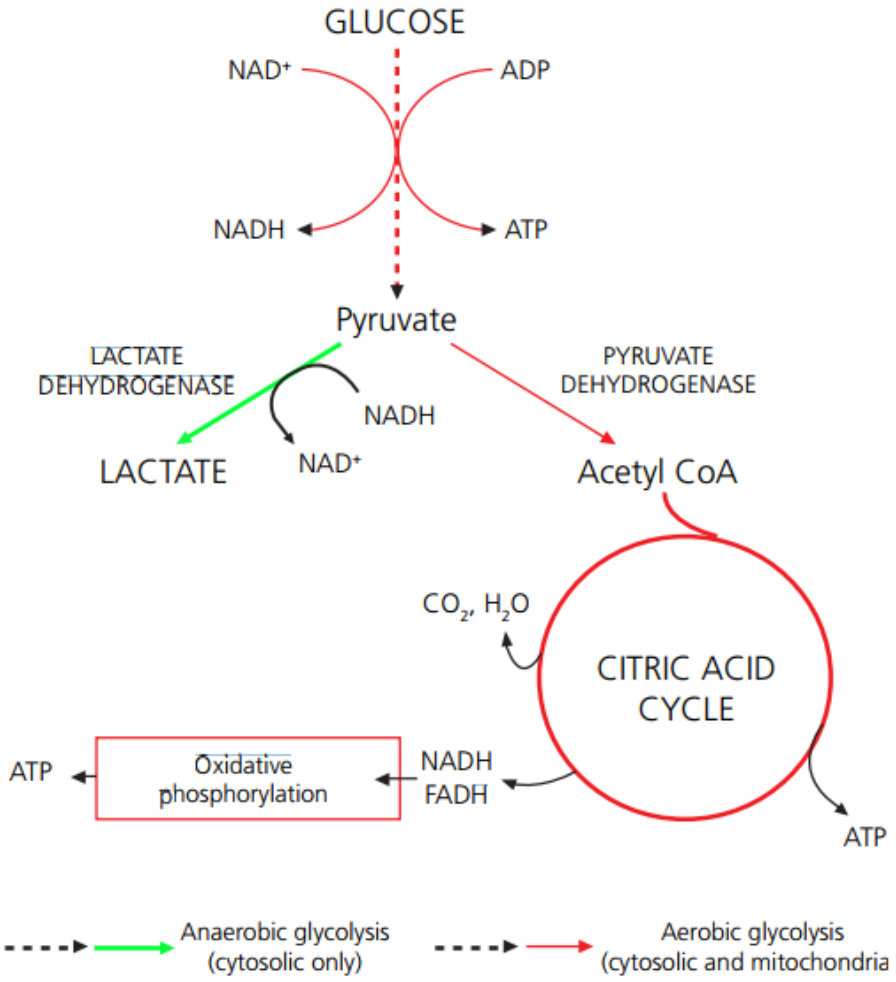

Figure 4 Glucose Metabolism with lactate as by-product [14]

The anaerobic metabolic pathway takes place in the cytoplasm of the cell. This conversion from glucose to pyruvate consists of a sequence of 13 enzymatic reactions. Whereas, energy-rich adenosine thriphosphate (ATP) is formed from adenosine diphosphate (ADP) and the reduced adenine dinucleotide (NADH) is generated from NAD^+, which is an oxidized NAD. The last step for lactate generation includes the converting process from pyruvate to lactate, which is performed by the enzyme lactate dehydrogenase. Within this final step NAD^+ is

formed that is necessary for the anaerobic glycolysis. In addition, lactate production is the only way to metabolize glucose producing energy in the erythrocytes, which have no mitochondria as well as in exercising muscle cells, which have an oxygen debt. [14]
The aerobic pathway on the other hand is dominant for well-oxygenated tissue cells that contain mitochondria. It is normally the preferred way to metabolize pyruvate through the Krebs cycle and oxidative phosphorylation. Within the aerobic glycolosis pathway a high amount of 38 ATP molecules are generated. The lower energy anaerobic pathway can also be performed in cells without any mitochondria (erythrocytes) and skeletal muscles, which have an oxygen deficiency. Only 2 ATP molecules are generated and therefore is much less effective [14].

4.2.2 Lactate removal

The disposal of lactate has two main routes: Firstly conversion back to pyruvate and secondly, excretion in urine, which only makes up about 2% of total lactate disposal. The remaining 98% of lactate converts cytosolic to pyruvate by the enzyme lactate dehydrogenase. The newly generated pyruvate can also take further two pathways. First option is the citric acid cycle to produce ATP again, the second one is gluconeogenesis. Within this chemical process, pyruvate converts to oxaloacetate and ultimately ends in glucose. The gluconeogenesis only appears in kidneys and in livers. **Figure 5** shows the whole degradation process [14].

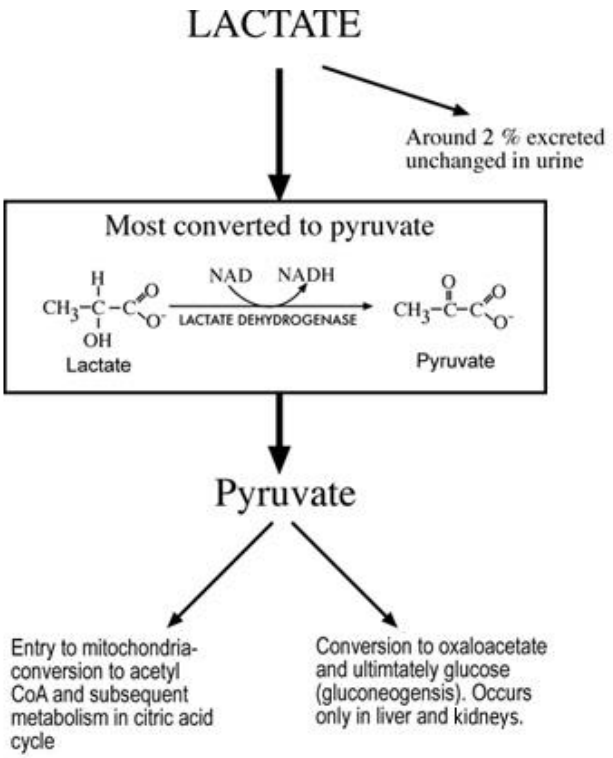

Figure 5 Lactate removal in the human body [14]

4.2.3 Health risks through Lactate

Constantly elevated blood lactate levels can lead to further health risks. This medical phenomenon is called hyperlactatemia or lactic acidosis and can be divided into two broad categories, Type A and Type B. Hyperlactatemia Type A involves an absolute or relative hypoxemia, which means an abnormally low level of oxygen in the blood because of anaemia or increased muscle activity. For type B lactic acidosis there is no evidence of hypoxemia. This type only arises with underlying diseases such as cancer or severe liver failure [11]. Within these categories septic shock may lead to type B. Shock currently is conceptualized as a clinical syndrome resulting from an imbalance between tissue oxygen demands and tissue oxygen supply. It is believed that the produced amount of lactate correlates with the total oxygen debt and the severity of shock [9]. A too high amount of lactate in the blood can lead to death [10].

4.2.4 Lactate and other biological molecules spectra

The first part of this thesis involves finding absorbance spectra from lactate and further biological molecules, which have nearly the same chemical structure. Because of the related structure, the physical characteristics, especially the spectroscopic ones, are similar. **Figure 6** illustrates the first spectrum with glucose (black graph), lactate (dotted graph) and urea (grey graph). Despite all the structural similarities, the lactate peaks and the peaks of urea and glucose are not too close. The lactate peaks are at 4350, 4450 and 4800 cm^{-1} wavenumbers [15]. These wavenumber values correspond to wavelengths of 2299, 2247 and 2080 nm respectively. The last peak with 2080 nm is irrelevant for further observations, due to its broadness. Moreover the glucose absorbance is also higher at this point of the spectrum. Therefore results from this peak would not be reliable.

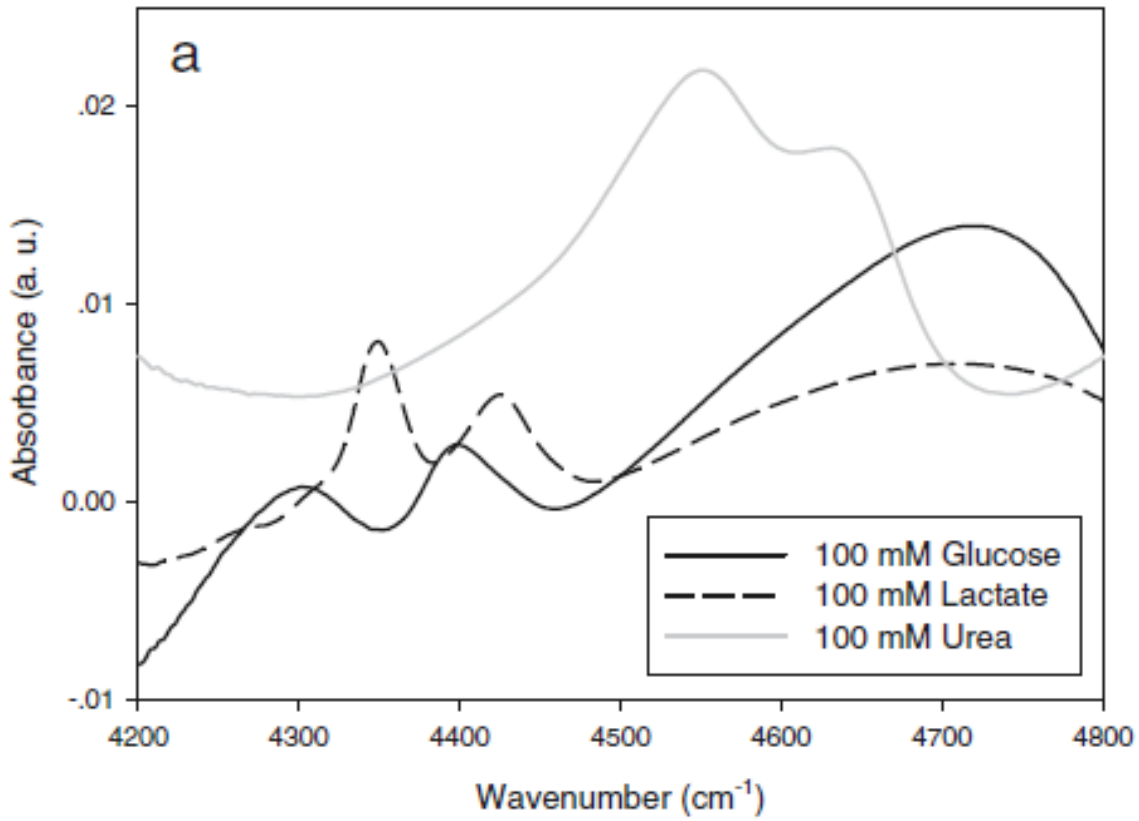

Figure 6 Spectra of lactate, glucose and urea according to literature [15]

Figure 7, shows the second spectrum with the same molecules and cholesterol and triacetin added. Cholesterol has a peak very close to the 4350 cm^{-1} lactate signal. Therefore it is extremely interesting for our further research. Triacetin, also called glycerol triacetate, is a

further molecule, which is mainly used in the pharmaceutical industry. It is an excipient and is especially used as humectant and solvent in pharmaceutical products [16]. However, triacetin is not included in this study, because it is not a naturally occurring biological molecule in the body. Another feature of this plot is the normalized absorbance, defining values between 0 and 1. This is done by dividing the spectrum by the maximum value for each biological molecule. For this reason there are always peaks at an absorbance value of 1.

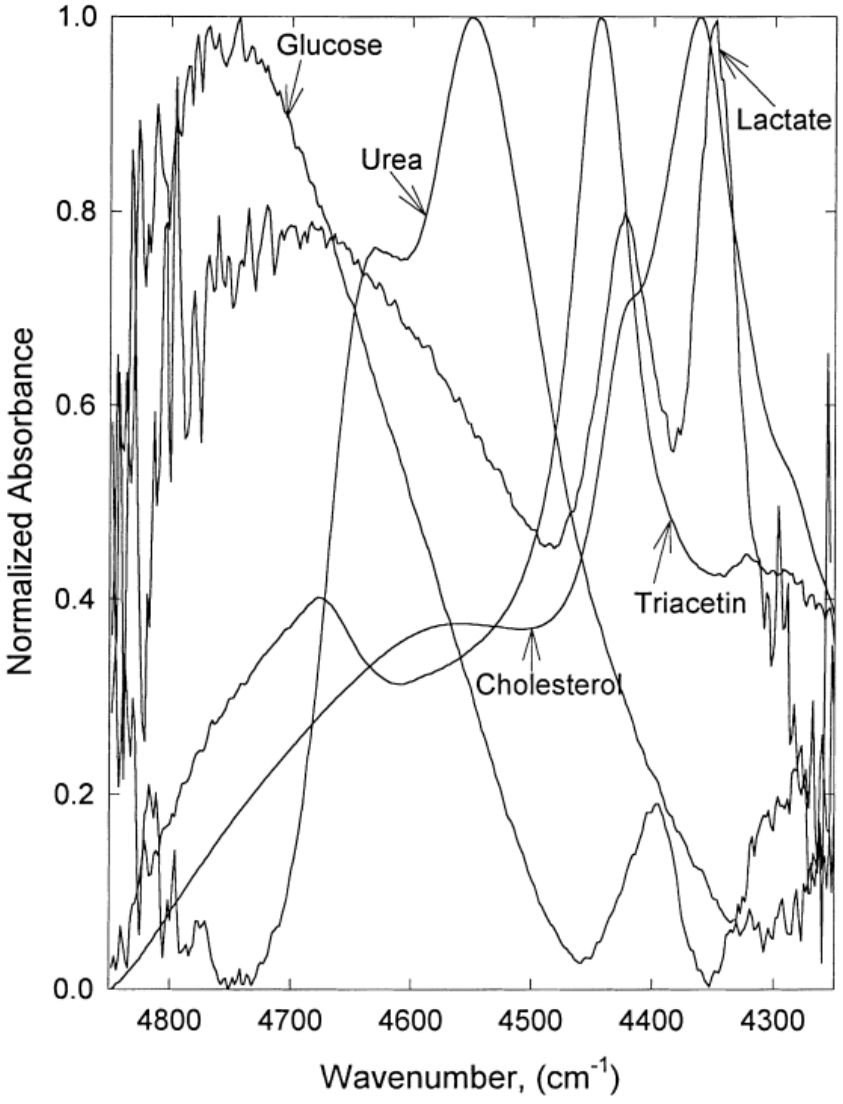

Figure 7 Spectra of lactate, urea, cholesterol, glucose and triacetin according to literature [17]

4.2.5 Other biological molecules

Urea

Urea is a nitrogen-containing substance and is essential for the N-metabolism. The structural formula of urea is $CO(NH_2)_2$. It is highly soluble in water and therefore normally cleared from the blood by the kidney into the urine. In addition, urine dissolved in water is neither alkaline nor acidic. Urea originates from the liver, where two ammonia NH_3 molecules combined with one carbon dioxide CO_2 are converted to urea [18]. With the urea cycle, the body excretes nitrogen. Blood levels of urea are measured with the so called blood urea nitrogen (BUN) test [18], [19]. Urea displays peaks at 2186 nm and 2151 nm, which are not interfering with the lactate peaks at 2247 nm and 2299 nm [15].

Glucose

Glucose, also known as dextrose is a monosaccharide. It has the formula $C_6H_{12}O_6$ and is present in the human blood. It is the source of energy for cell function and the regulation of its metabolism is essential [20]. The glucose peaks are of high interest. Even though the structure of glucose and lactate is similar, it should be possible to measure them separately, as glucose peaks are at 2326, 2273 and 2105 nm [15].

Cholesterol

Cholesterol is not soluble in water and causes therefore many health risks. Due to the insolubility, it behaves like plaques in the blood vessel and is the main reason for arteriosclerosis, leading to health threatening problems like heart attacks. The chemical composition of the steroid cholesterol is $C_{27}H_{46}O$ [21]. Most important are once again the Cholesterol displays peaks in the infrared region at 2267 nm and 2293 nm compared to those of lactate at 2247 nm and 2299 nm. Fortunately, the peaks of both biological molecules are sharp, especially the higher wavelength ones, allowing for independent measurements [22].

5 Simulation

As part of this master thesis, two different simulations were conducted. The spectroscopic measurement of lactate, urea, glucose and cholesterol was simulated with two different filters, which cover the region of interest. First, two bandpasses were used to exactly determine the spectra. In the second simulation an Etalon, which is also called "Fabry-Perot interferometer", was used. Finally, those two different filtering processes were compared to each other, in order to find the most precise approach. In the following chapters, these two types of filters are explained in more detail.

5.1 Bandpass

5.1.1 Methods

The used bandpass filter belongs to the optical filters. Those have the ability to selectively transmit or reject a wavelength or range of wavelengths of incident radiation. Medicine, physics and chemistry are just some application fields which use the narrowing effect. Within those disciplines, methods are fluorescence microscopy, spectroscopy or machine vision inspection. In particular life science and imaging industry profit from these filter types [23]. To conduct the simulation, two optical bandpass filters have been designed in such a way, that they transmit a section of the spectrum, and block all other wavelengths. The data of those two bandpasses was obtained from the company "Thorlabs Inc.". The aim is to measure the lactate peaks at 2249 nm and 2299 nm. Therefore bandpasses which can detect those wavelengths, were required. In addition, they were also used to narrow the bandwidth of the filter. **Figure 8** illustrates the transmission of the two different bandpass filters and the combination of both as a function of the wavelength. The first bandpass has his centre wavelength at 2250 nm (blue graph) and the second one has it at 2500 nm (red graph). Combining both chosen filters leads to a narrowed bandwidth, as desired (yellow graph). A side effect of the described narrowing is a decrease in transmission intensity.

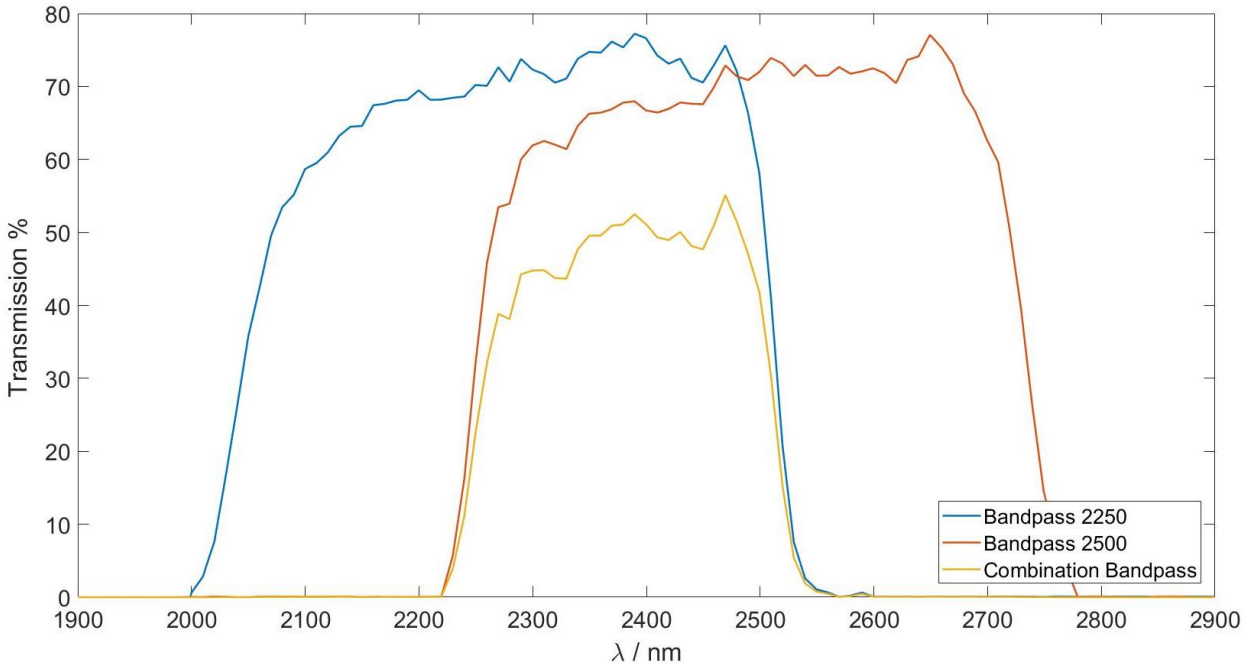

Figure 8 Bandpasses with a centre wavelength of 2250 nm (blue graph) and 2500 nm (red graph) and combination of both (yellow graph)

The next simulation step was to filter the lactate absorption spectrum. Therefore, the combined bandpass and the already measured sodium-L-lactate absorbance spectrum from the pure powder were used. This spectrum was directly obtained from Sodium-L-Lactate in powder form.

5.1.2 Results

This chapter covers the resulting sodium-L-lactate signal after filtering it with 2 band passes. **Figure 9** illustrates the measured sodium-L-lactate spectrum depending on the combined bandpass. In addition, the multiplication of the combined bandpass (blue graph) and the measured lactate (purple graph) yields the lactate referring to the bandpass (green graph).

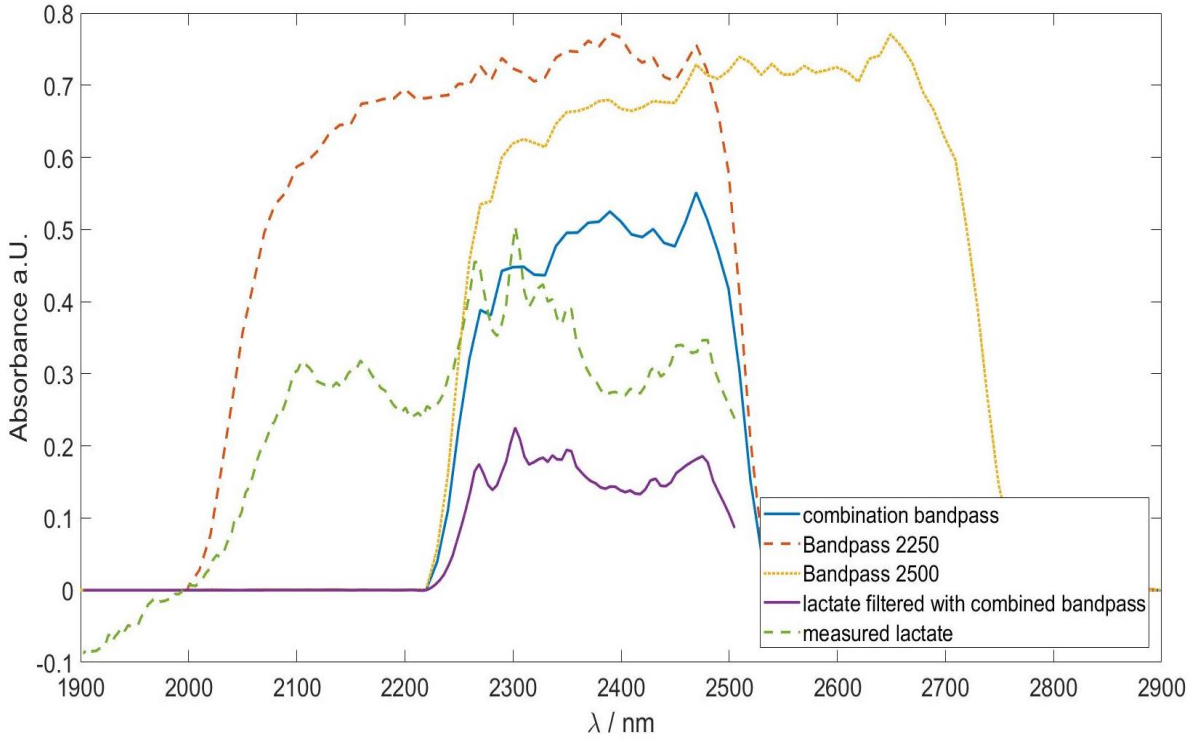

Figure 9 Measured Lactate (green graph) referred to combination bandpass (blue graph) and the result (purple graph).

Further, the spectrum of all four observed biological molecules was measured. Consequently, **Figure 9** shows the combination bandpass filter with all four molecules: lactate, urea, glucose and cholesterol. The blue graph depicts the combination bandpass filter, whereas the red graph is the fusion of all four molecules. As above already mentioned, the intensity decreases with every multiplication. Accordingly, the correlation of the molecules with the combined bandpass (yellow graph) refers to a lower intensity as the combination bandpass.

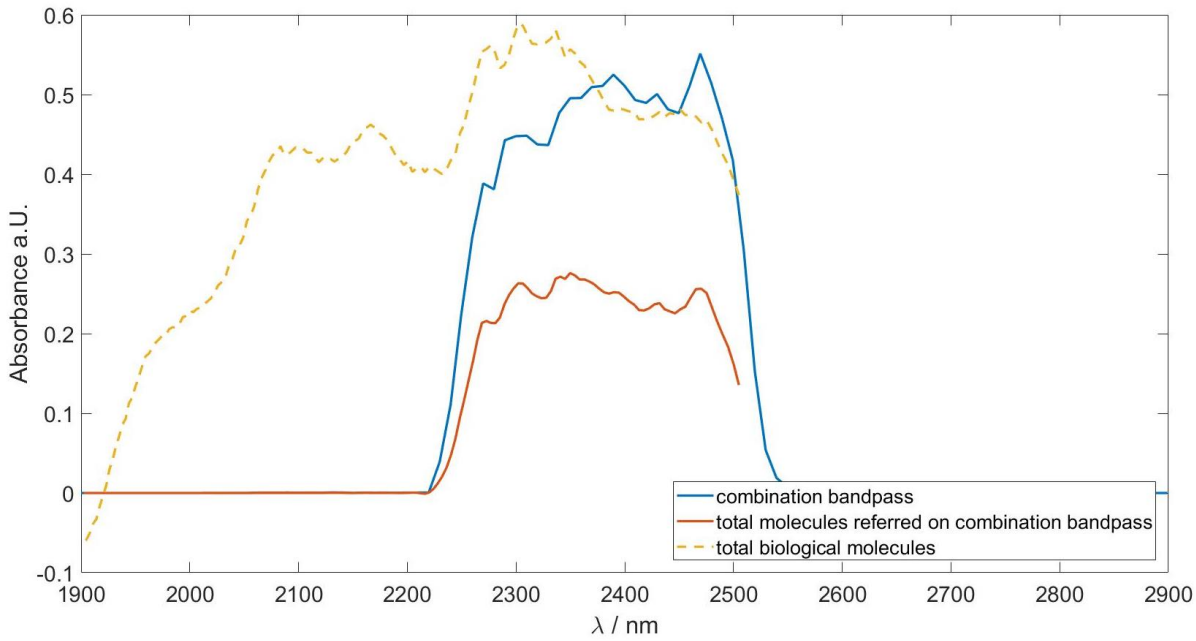

Figure 10 All 4 biological molecules combined (yellow graph) filtered with the combined bandpass (blue graph) results in the red graph

5.1.3 Discussion

As pictured in **Figure 10**, every multiplication leads to an intensity loss. Nevertheless, the two lactate peaks at 2249 nm and 2299 nm can be identified and therefore the method can be used to measure those peaks. Although, the combination bandpass is a good narrowed filter, it is not the best solution because the measurement is difficult, especially if other biological molecules are present. In comparison to the **Figure 9**, the lactate peaks cannot be identified as easy as above. Therefore, this simulation set up is not suitable to identify the lactate peaks in attendance of other biological molecules. As a result, we need a better option to determine the lactate peaks. The solution to meet this scope was the use of an Etalon.

5.2 Etalon

5.2.1 Theory

The Fabry-Perot Interferometer, which is also called Etalon, was invented by C. Fabry and J.-B. Perot in 1900. The Etalon is an interferometer which uses the effect of multiple beam interference and consists of two planar glass plates, which are arranged in parallel at a distance, see **Figure 11**. Those two terminologies, Etalon and Fabry-Perot Interferometer are often used inconsistently, but there is a slight difference. An Etalon is manufactured with highly reflective glass plates which are often smoothed. For this experiment an Etalon was used. To vary the filtered wavelength, the distance between those two plates can be adjusted. Furthermore, the reflecting part of the plates must possess a high amount of planarity, with deviations smaller then $\lambda/20$ and coated plates being permissible. The design configuration of an etalon is illustrated in **Figure 11**. An Etalon consists of a socket, an end ring, a small air gap within the physical process takes place, a compensation ring, a spring and tuning screws [24].

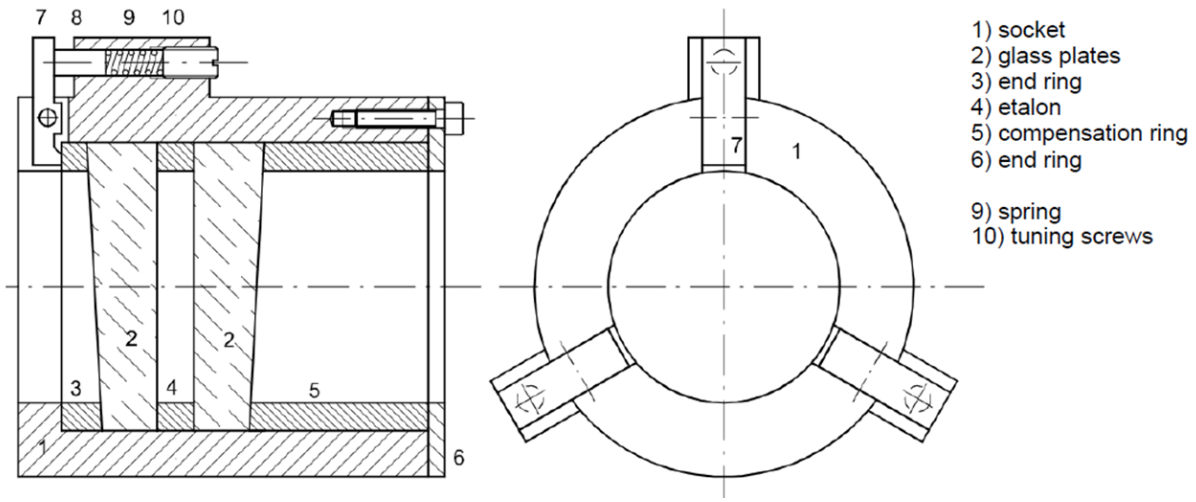

Figure 11 Etalon setup [25]

An impinging light ray on the first mirror is transmitted to the second one and gets reflected several times in between those two mirrors. Just a small amount transmits the interferometer and can be captured with an appropriate lenses combination [24]. **Figure 12** pictures the principle behaviour of the light in an etalon.

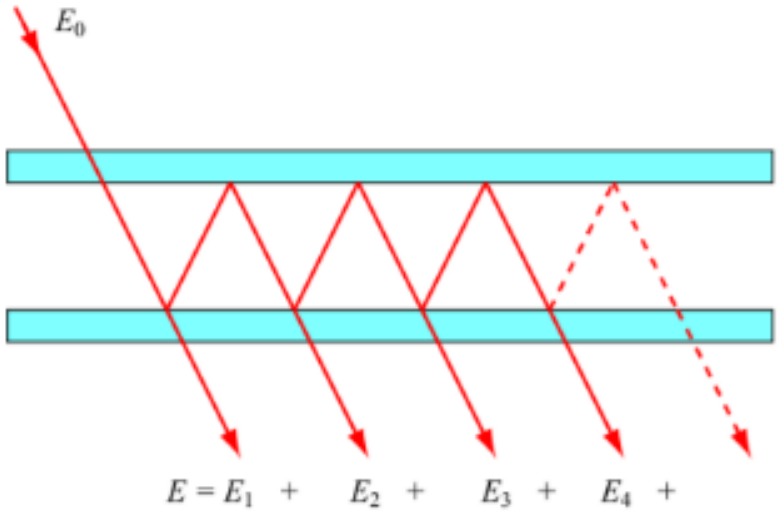

Figure 12 Principle behaviour of the light in an Etalon [26]

The transmitted light depends on the distance l of the Etalon also called thickness, the wavelength λ of the used light beam, the refraction index n from the material of the Etalon and the angle Θ [24]. In detail, the interference between the multiple reflections of light causes a varying transmission function. To identify the peak, the transmitted beams must be in phase, this leads to a so called constructive interference. On the contrary, a destructive interference occurs if the transmitted beams are not in-phase, this would induce a minimum transmission. Whether constructive or destructive interference happens, depends on the wavelength λ of the applied light, the refractive index n of the material, the thickness of the etalon l and the angle Θ the light travels through it, as shown in the **Figure 13** [24] [27].

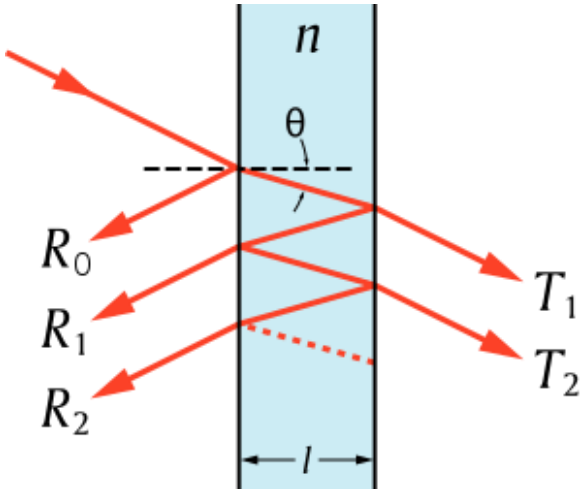

Figure 13 Principle behaviour of the light depending on the parameters [27]

The formula (1) for the phase difference (T2-T1 in **Figure 13**) is given by δ. It is directly proportional to the refractive index n and the thickness of the Etalon l and indirect proportional to the wavelength λ [27].

$$\delta = \left(\frac{2\pi}{\lambda}\right) 2 \cdot n \cdot l \cdot cos(\theta) \tag{1}$$

In this simulated experiment, the angle is 0° or 360°, because the light irradiates directly on the surface. As a result, the above-mentioned formula is reduced to the following (2)(3):

$$cos(\theta) \equiv 1 \tag{2}$$

$$\delta = \left(\frac{2\pi}{\lambda}\right) 2 \cdot n \cdot l \tag{3}$$

The main parameter to be measured was the transmittance of the Etalon T_e for lactate. Within the transmittance, the reflectance R must be defined, which is the ratio between the intensity of reflected radiation and the radiation incident on a surface [28]. The formula for the transmittance is given by (4):

$$T_e = \frac{(1-R)^2}{1 - 2\,R\,cos(\theta) + R^2} \tag{4}$$

Another important parameter is the finesse *F*. It describes the sharpness of the filter. The smaller the finesse gets, the wider the filter gets for the peaks. Vice versa, the larger the finesse the sharper the filter gets for the peaks. It only depends on the reflectance, as shown in formula (5). Noteworthy, there is no dependency on the wavelength.

$$F = \frac{4\,R}{(1-R)^2} \tag{5}$$

There is also a possibility to describe the transmittance of the etalon T_e with the finesse:

$$T_e = \frac{(1-R)^2}{1 - 2\,R\,\cos(\theta) + R^2} = \frac{1}{1 + F\,\sin^2\left(\frac{\delta}{2}\right)} \tag{6}$$

In the conducted experiment, the transmittance was calculated using formula (6).

5.2.2 Calculation / Methods

The next step is to calculate the ideal thickness L to measure lactate peaks at 2247 nm and 2299 nm. The ideal coating for measurements in the near-infrared region is fused silica. For the first peak of 2299 nm the refractive index n_1 is 1.4334 by fused silica and for the second peak of 2247 nm n_2 is 1.4342. These two formulas are given by (7) (8).

$$L_1 = \frac{k \cdot \lambda_1}{2\, n_1} \tag{7}$$

$$L_2 = \frac{k + x \cdot \lambda_2}{2\, n_2} \tag{8}$$

In the considered case the Etalon should measure both peaks. Therefore, it is necessary to adhere to the following resonance condition (9) (10).

$$L_1 = L_2 \tag{9}$$

$$k, x \in \mathbb{Z} \tag{10}$$

Because of this resonance condition, the formulas for the thickness $L_1$and L_2 are equalized. Moreover, k (dependent on x) can be calculated, whereas x is an integer and the number of oscillation between two lactate peaks. The condition is fulfilled with an x value of 1 and a k value of 42. Hence, the thickness of the Etalon is 36 µm. In the figure below, you can see the simulated Etalon with those specifications and different finesse values. The finesse was set to a value of 5. Due to the smoothness of the lactate peaks it would not be reasonable to take a filter with a finesse of 50.

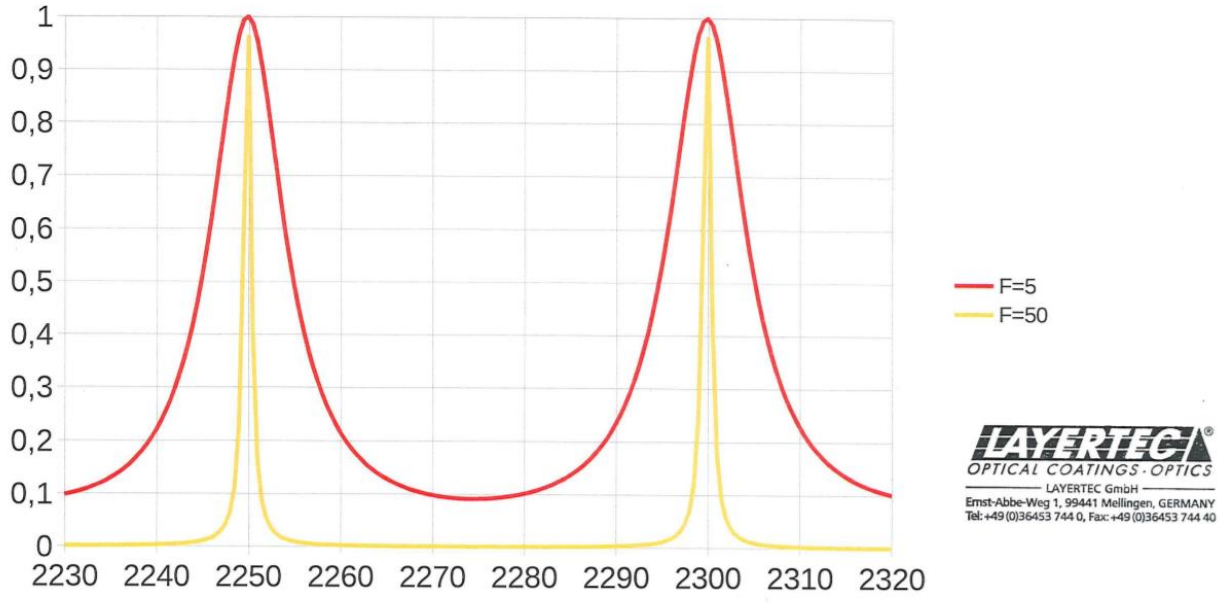

Figure 14 Etalon with a thickness of 36 µm and two different finesses: red graph (F = 5) and yellow graph (F = 50) [29]

The next figure illustrates the result of the simulation with the following values: $x = 6$ and $k = 253$. Therefore, the thickness has been calculated with 216 µm.

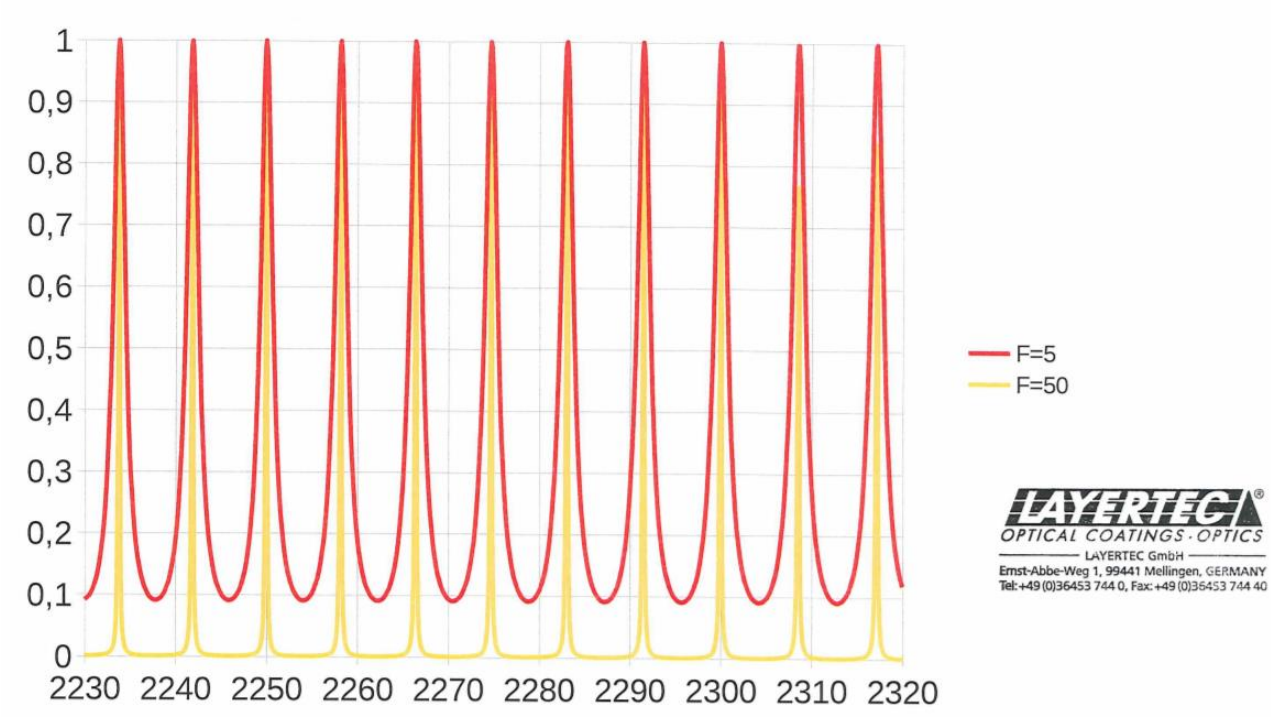

Figure 15 Etalon with a thickness of 216 µm and two different finesses: red graph (F = 5) and yellow graph (F = 50) [29]

5.2.3 Results

To choose the best fitting thickness L, a simulation in MATLAB has been performed. As input data the combined spectrum of all four biological molecules with the two thickness options were used. The data for the combined molecule spectrum originates from the literature reference [17]. The first plot (**Figure 16**) shows the thin etalon spectrum with 36 µm (red graph) and the combined spectrum of the four biological molecules: lactate, urea, cholesterol and glucose (blue graph). The two peaks of interest did not get hit at the highest point (see red circles). Therefore, the filter is not ideal for this measurement.

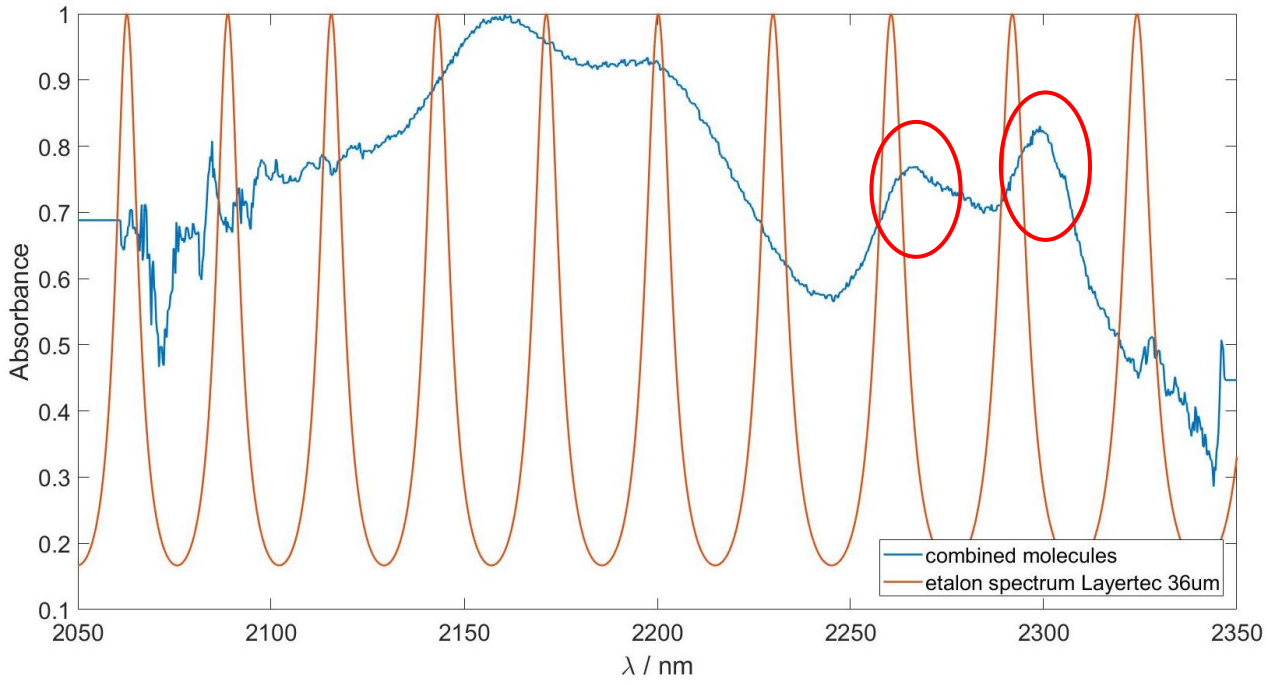

Figure 16 Etalon with a thickness of 36 µm with a finesse of 5 (red graph) and combined molecular spectrum (blue graph)

Secondly, the plot of the Etalon with 216 µm is pictured in the **Figure 17**. The etalon spectrum 216 µm (red graph) is - compared to **Figure 16**- sharper and does sense more peaks correlating to the higher x value. The blue graph is again the combined biological molecule spectrum. Now, the Etalon spectrum filter encounters the peaks of the combined biological molecules precisely. Therefore, the decision to take the Etalon filter with the thickness of 216 µm was made. Not only is the result better, but it is also a lot easier to manufacture. Thicknesses of under 34 µm are nearly impossible to confect at a reasonable price.

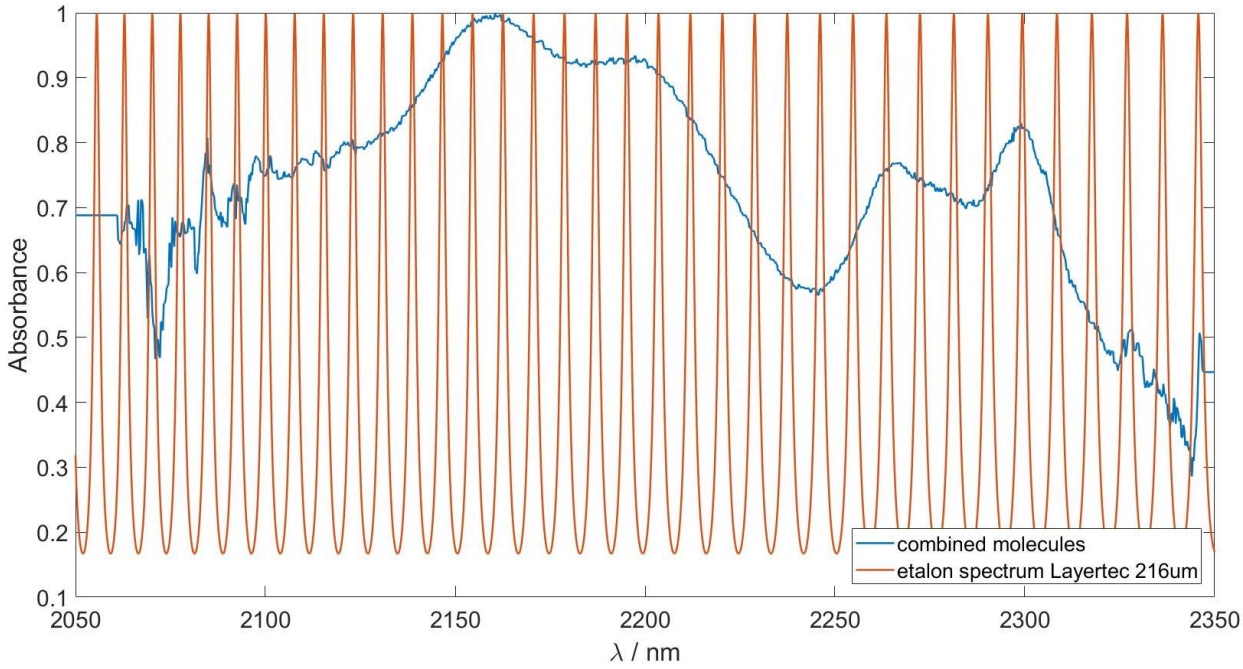

Figure 17 Etalon with a thickness of 216 µm with a finesse of 5 (red graph) and combined molecular spectrum (blue graph)

With the selected Etalon thickness of 216 µm as filter, each biological molecule was plotted separately. **Figure 18** displays the etalon spectrum (blue graph), the lactate spectrum (purple graph), the urea spectrum (red graph), the glucose spectrum (yellow graph) and the cholesterol spectrum (green graph). Notably, the filter matches the peaks of the lactate spectrum precisely, whereas the other compounds are not matched as precisely. For this reason, the etalon with a thickness of 216 µm is a good filter to measure just the lactate peaks in presence of other biological molecules.

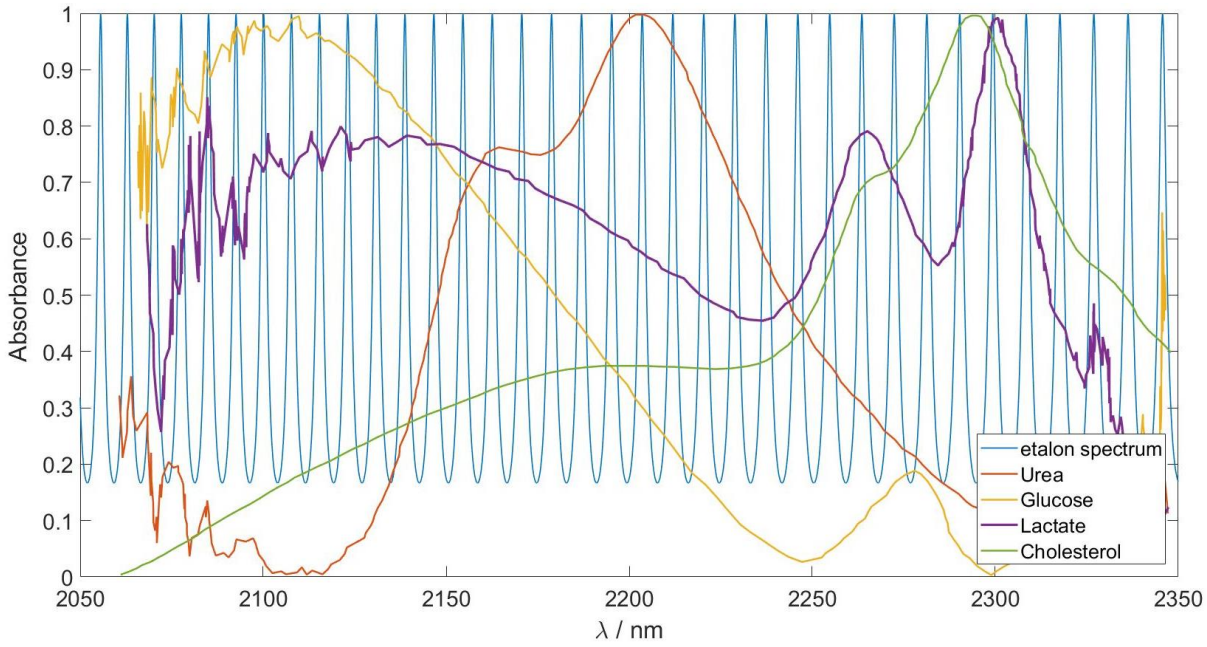

Figure 18 Etalon with a thickness of 216 µm (blue graph) with the 4 molecular spectra

5.2.4 Discussion

Both filter types, 2 bandpass filters and an Etalon are able to measure the lactate peaks. The bandpass filter measures a whole spectrum band and in the presence of other biological molecules there is no separation possible, which can be solved using an Etalon. In addition, the thickness parameter L is very important for the etalon, due to the correlation with the wavelength. The perfect sampling of the peaks was achieved at a thickness of 216 µm.

6 Measurements with Spectrometry

6.1 Theory

6.1.1 Transmission

The transmission T is a parameter, which describes a body's permeability towards light and can be calculated with the following formula (11) [30].

$$T = \frac{I}{I_o} \tag{11}$$

Whereas,

I…… transmitted light

I_0….. incident light

6.1.2 Absorption

Absorption describes the ability of a substance to absorb a wave or a particle, for instance infrared light which consists of photons [31].

$$\frac{I}{I_0} = e^{-\mu d} \tag{12}$$

Whereas,

I…… transmitted light

I_0….. irradiated light

μ…… attenuation coefficient

d…… thickness of the material

6.1.3 Absorbance

Absorbance measures the ability of a refractive medium or optical component to absorb light. Therefore it determines how much light is lost when it travels through the given medium. Both, scattering and refraction of light, are taken into consideration. The absorbance A can be described as the logarithm (base 10) of the reciprocal of the transmittance: [30]

$$A = 10 \cdot log_{10}\left(\frac{1}{T}\right) \tag{13}$$

Absorption spectroscopy is typically used to measure the absorbance of a dissolved substance. Light shines through the solution onto a detector, which records how much light and at which wavelengths was transmitted [32] [33].

6.1.4 Lambert-Beer Law

This law describes the linear relationship between absorbance and concentration of an absorbing species and follows the formula (14) [34].

$$E_\lambda = log_{10}\left(\frac{I_o}{I_1}\right) = \varepsilon_\lambda \cdot c \cdot d \tag{14}$$

Whereas,

E_λ……. Extinction

I_o ……. Intensity of the incident light in $\mathrm{W \cdot m^{-2}}$

I_1…….. Intensity of the transmitted light in $\mathrm{W \cdot m^{-2}}$

ε_λ……..decadal extinction coefficient in $\mathrm{mol^{-1} \cdot m^2}$

c……molar concentration in $\mathrm{mol \cdot l^{-1}}$

d……. Thickness of the irritated body in m

For my experiments, the thickness d is an important parameter. The higher the thickness gets, the less light is transmitted through the fluids. Particularly water is absorbing a lot of light. For this reason a MATLAB plot was created, see **Figure 19**, where this physical phenomenon of water is illustrated. The wavelength region of interest is the region between 2000 and 2500 nm. Within this values all our four biological molecules' peaks exist. In this section between 2000 nm and 2500 nm water does not absorb everything and therefore absorbance measurements are possible. The biggest diameter which still transmits light, is 0.2 cm (purple graph). At higher thicknesses, water absorbs all light.

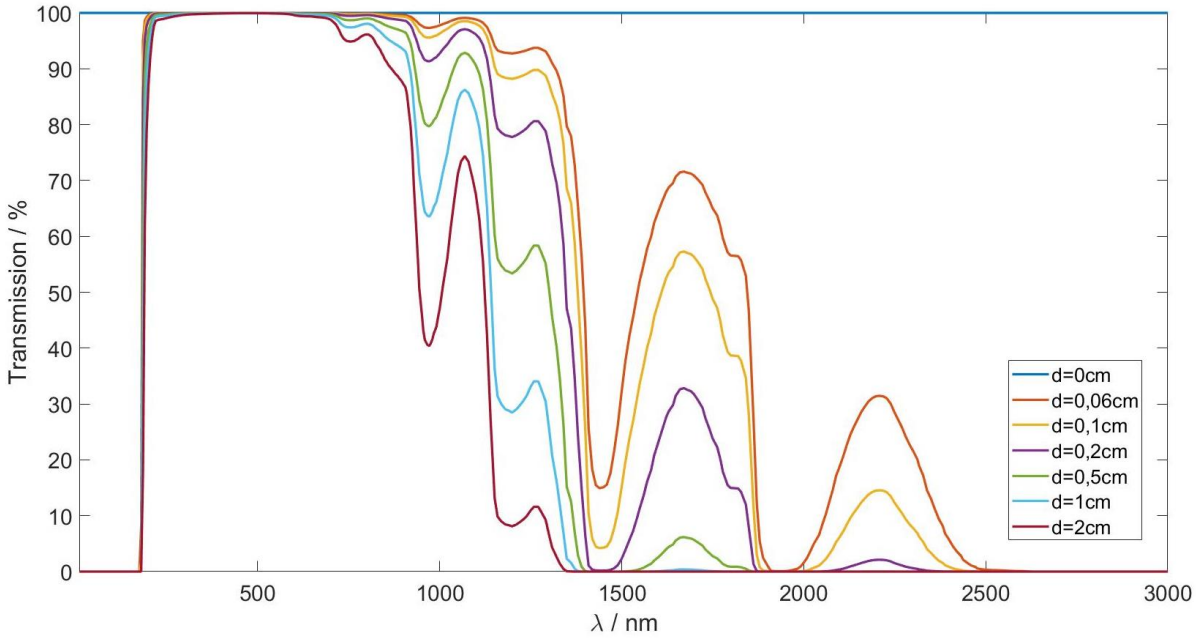

Figure 19 Lambert Beer Law: the amount of transmitted light is inversely proportional to the depth of the irradiated solution (water)

6.2 Methods

For the spectrometry measurement the Arcspectro FT Rocket Fourier- Transform Spectrometer was used, which is able to determine spectra in the infrared region. The spectrometry is quite a simple method to get the absorbance spectrum of a molecule, but a huge drawback is that it is expensive and big as well. The result is that there is no simple home application possible.

First, the spectrum of the powder with the spectrometer of all four biological molecules have been measured. Those results have also been used for the simulation topic as previously mentioned. **Figure 20** illustrates the sodium-L-lactate (blue graph), cholesterol (red graph), glucose (yellow graph) and urea (purple graph) spectrum. Specifically the lactate peaks at 2247 and 2299 nm are of interest for this experiment, which are distinct.

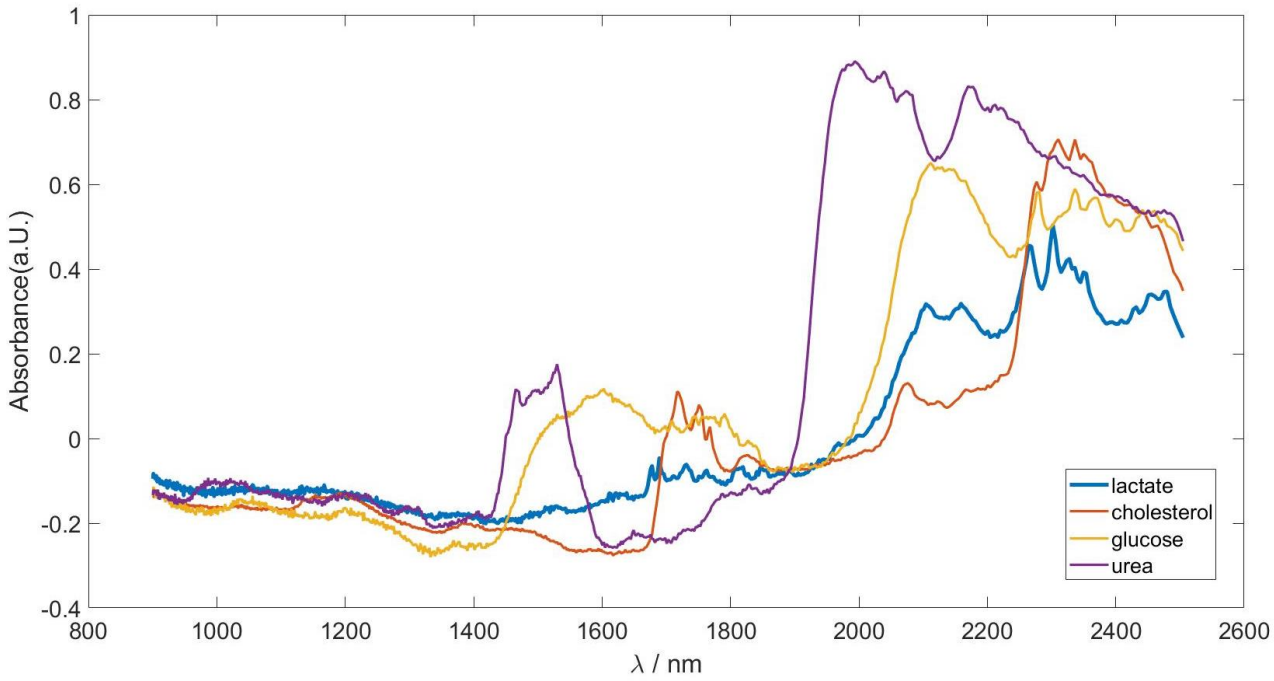

Figure 20 Measurement of all four biological molecules: lactate (blue graph), cholesterol (red graph), glucose (yellow graph) and urea (purple graph) in powder form

The next step is to measure the blood concentrations of all four biological molecules. The powders have to be dissolved in distilled water. The different blood concentrations are 5-20mg/dl for lactate, 12.84-42.8 mg/dl for urea, 70-110 mg/dl for glucose and <200 mg/dl for cholesterol. Lactate was added as sodium-L-lactate. In the end, three sodium-L-lactate concentrations were mixed. The first two sodium-L-lactate concentrations correspond to the blood values, the last one was chosen according to a paper that measures with 1,12g/dl (=100 mmol/l) [15]. For the other three molecules only the highest blood concentration was measured. Final measured concentrations are listed in the following **Table 2**.

Table 2 Measured concentrations of sodium-L-lactate, urea, glucose and cholesterol

Biological molecule	Concentration
Sodium L-Lactate	6 mg/dl
	25 mg/dl
	1,12 g/dl
Urea	42 mg/dl
Glucose	110 mg/dl
Cholesterol	200 mg/dl

In addition, the measured spectrum of those concentrations were compared to the powder spectrum.

6.2.1 Measuring setup

For this measurement a special setup was inevitable. The components are a spectrometer, a broadband light source, a fibre and a containment for the solution. The used RP30 fibre is specialized to measure in the near-infrared region. **Figure 21** shows the experimental setup.

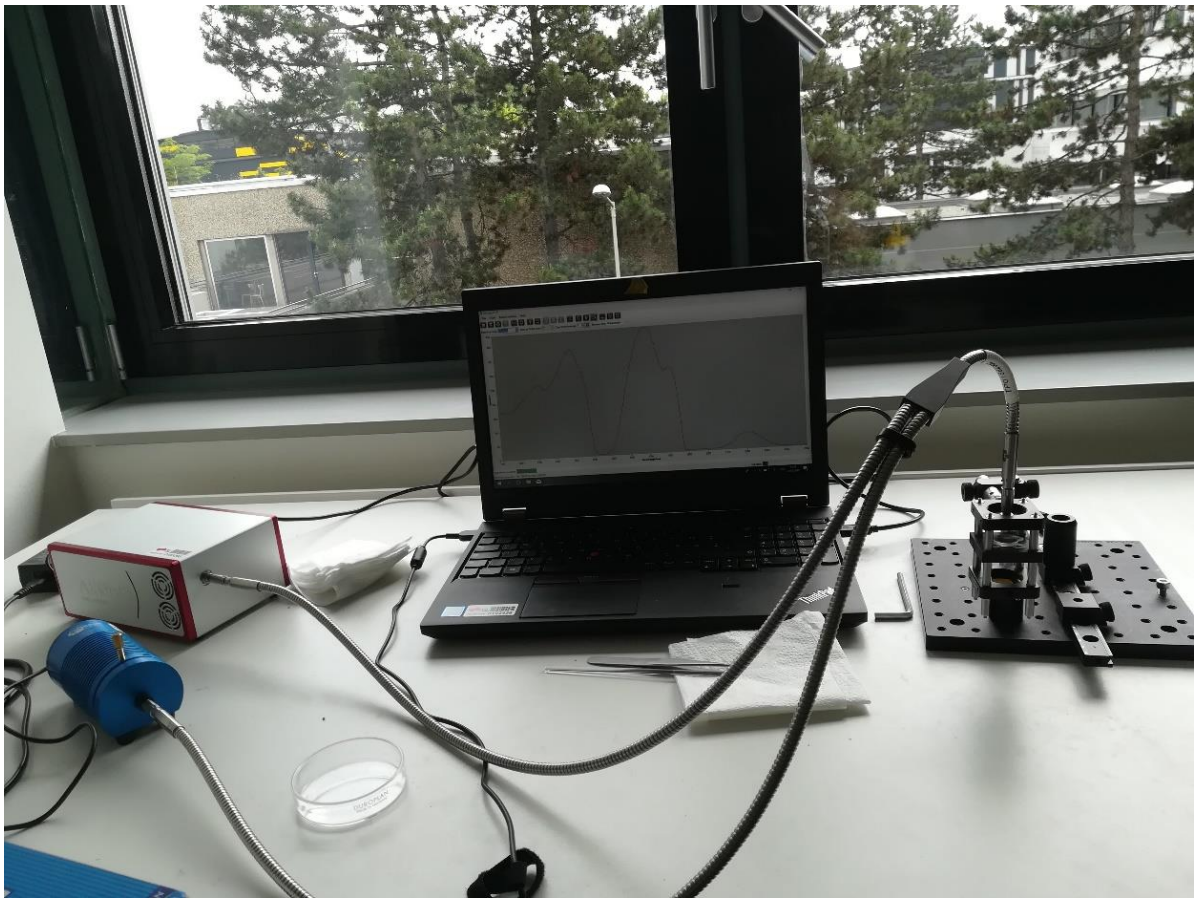

Figure 21 Measuring setup consisting of a spectrometer, a broadband light source, a RP30 fibre and a laptop

For solution containment two sapphire glass plates were used, with spacers to separate them. With these components it is possible to create a cuvette with a certain solution height. Volume is secondary, as the height is always reached at the centre of the high surface tension droplet and was adjusted to allow for unhindered measurement. **Figure 22** illustrates this solution holding setup. The sapphire glass is permeable to infrared light.

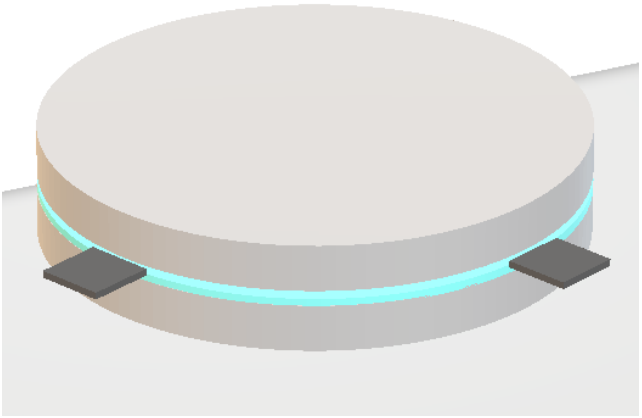

Figure 22 Solution holding setup consisting of two sapphire glass plates, four spacers and the solution

At the bottom of the solution holding setup a concave spherical gold mirror was attached to reflect all the transmitted light of the solution back to the fibre. In the fibre tip, which acts as in- and output, the determination of the absorbance spectrum continues. **Figure 24** pictures the whole solution holding setup. In addition, to hold that sapphire glasses and solution construction a 3D-printing in SolidWorks was designed. Due to the instability of the measurement setup, it was necessary to take further steps to guarantee the repeatability and the reproducibility of the experiment. Therefore, to eliminate any outliers each measurement was repeated 10 times and afterwards the mean and the standard deviation with a confidence interval (Student's t-quantile) of 95 % was calculated. See **Figure 23** for the measurement series of sodium-L-lactate 25 mg/100 ml with the 0.3 mm gap.

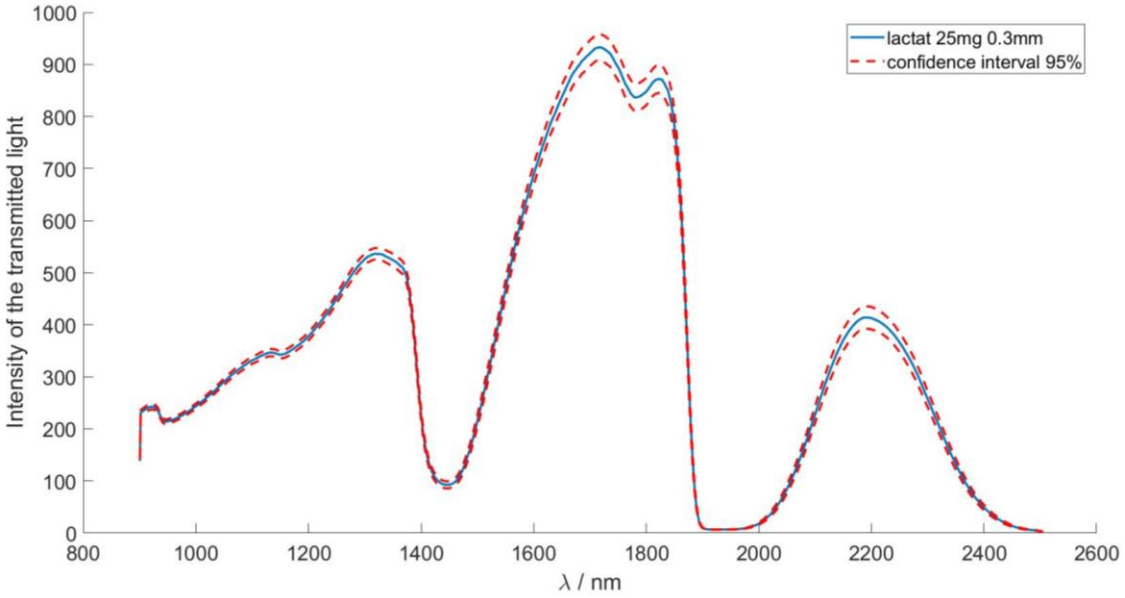

Figure 23 Mean value (blue graph) of the measured intensity of the transmitted light of sodium-L-lactate 25 mg/100 ml with a 95% confidence interval (red graph)

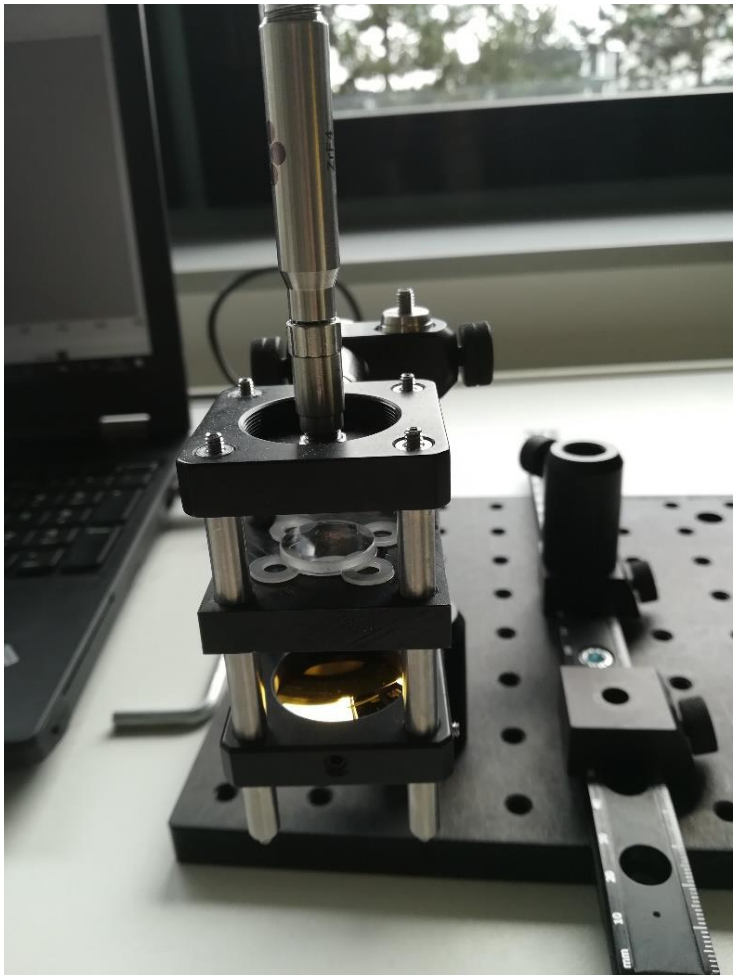

Figure 24 Solution between two sapphire glass plates with a gap of 1mm

First, the measurement was performed without spacers. However all measurement results were almost the same, no matter how high the concentration was or which molecule was determined. Only very small changes were recognizable. Initially, use of a highly concentrated 100 mmol/l solution, as suggested in the literature [15], was attempted. However, no improvement was achieved. Hence, a larger amount of solution was used. This was achieved with the spacers in between the sapphire glass plates. The first spacers were silicium lamellas (d=0.3 mm) and the second were plastic lamellas (d=1 mm). As a result we get three different measuring setups with 0 mm, 0.3 mm and 1 mm

Figure 25 and **Figure 26** shows these different gaps.

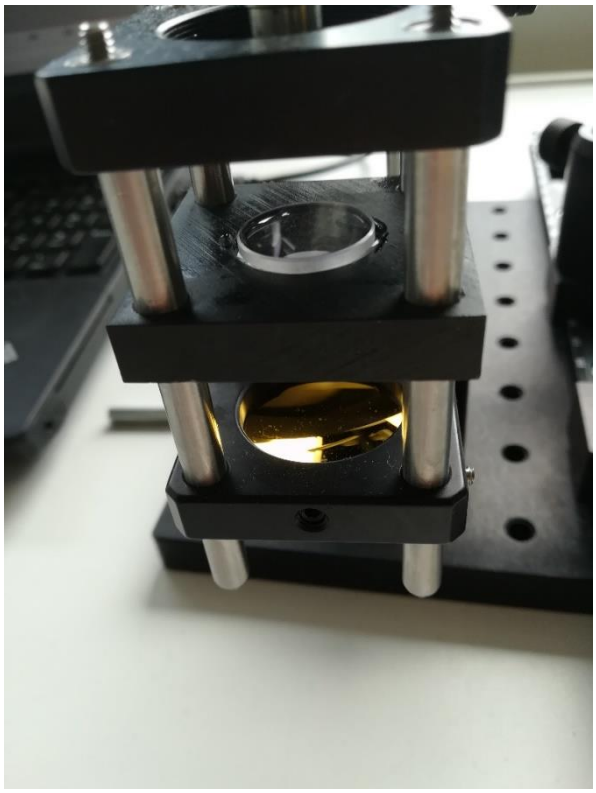

Figure 25 Solution between two sapphire glass plates with a gap of 0mm

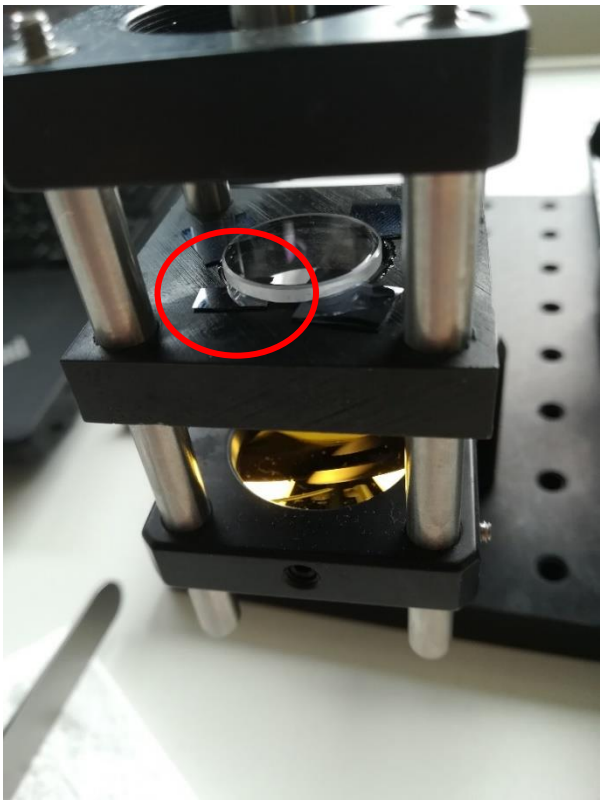

Figure 26 Solution between two sapphire glass plates with a gap of 0.3mm

As already mentioned, every single concentration was measured with three different depths of solution. **Table 3** summarizes the gap sizes and in addition the quantity of the solution.

Table 3 Correlation between depth and volume of solution

Depth of solution	*Volume of solution*
~ 0 mm	5 µl
0.3 mm	10 µl
1 mm	20 µl

Due to the fact that the spectrometer fibre irradiates and also absorbs the light, the light path is double the length and consequently the measured distances have to be taken double to get the right result. **Table 4** represents the correlated distances with the light path.

Table 4 Correlation between depth and volume of solution for the case of the double light path

Depth of solution	*Volume of solution*
~ 0 mm	5 µl
0.6 mm	10 µl
2 mm	20 µl

6.3 Results

The main focus was to determine the sodium-L-lactate concentration which was measured with three different concentrations. **Figure 1** shows the MATLAB plot of the lowest measured sodium-L-lactate concentration (6 mg/100 ml). This is equivalent to the minimum blood concentration of lactate of 5 mg/100 ml. This measurement was performed with the three different layer thicknesses of the solution: 0 mm, 0.3 mm and 1 mm. The plot pictures those three different volumes of solutions compared to the absorbance spectrum of sodium-L-lactate in powder form (purple graph). The yellow graph, which corresponds to the 1 mm gap, provides the best fit and it is possible to define the two lactate peaks at 2247 nm and 2299 nm.

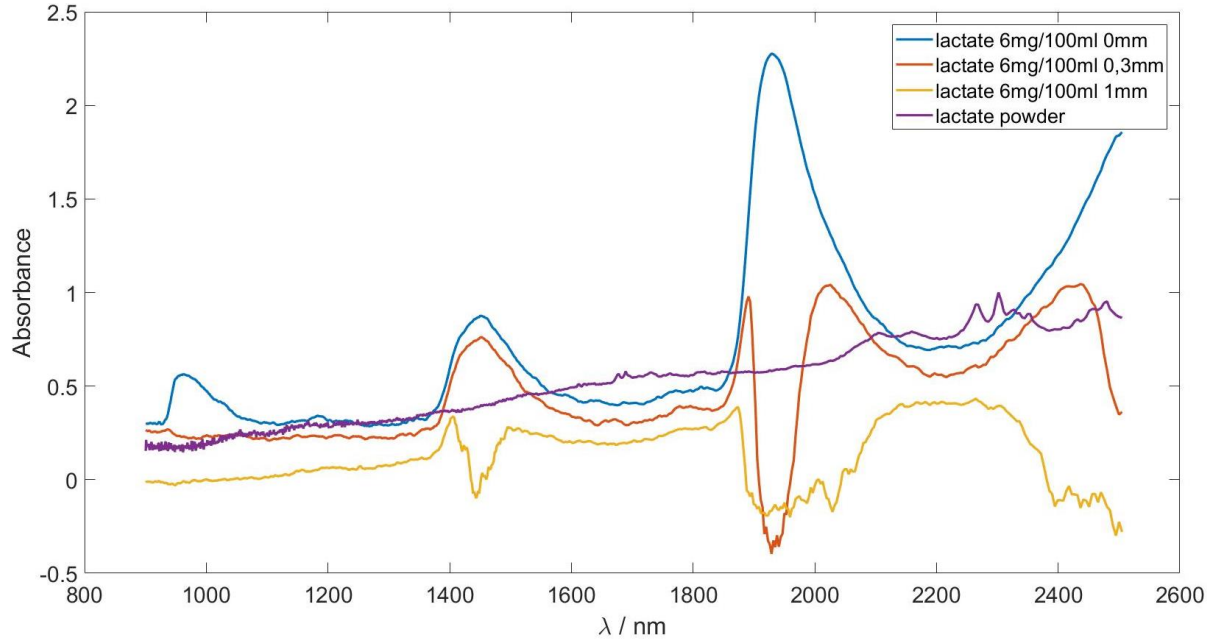

Figure 27 Absorbance of lactate 6 mg/100ml with solution depths of 0 mm, 0.3 mm and 1 mm and lactate powder

The next step is to compare the sodium-L-lactate 6 mg/100 ml with the 1 mm gap which seems the best fit with the lactate powder. **Figure 28** illustrates the comparison by superposing those two graphs. The blue graph shows the lactate and distilled water solution and the red graph represents the absorbance spectra of the pure lactate powder. The two peaks fit perfectly the two more distinct peaks of the pure sodium-L-lactate powder. In addition there is an obvious difference between the two graphs at 1450 nm, 1900 nm and after 2400 nm. These regions display exactly the water absorbance peaks, which have already been mentioned earlier.

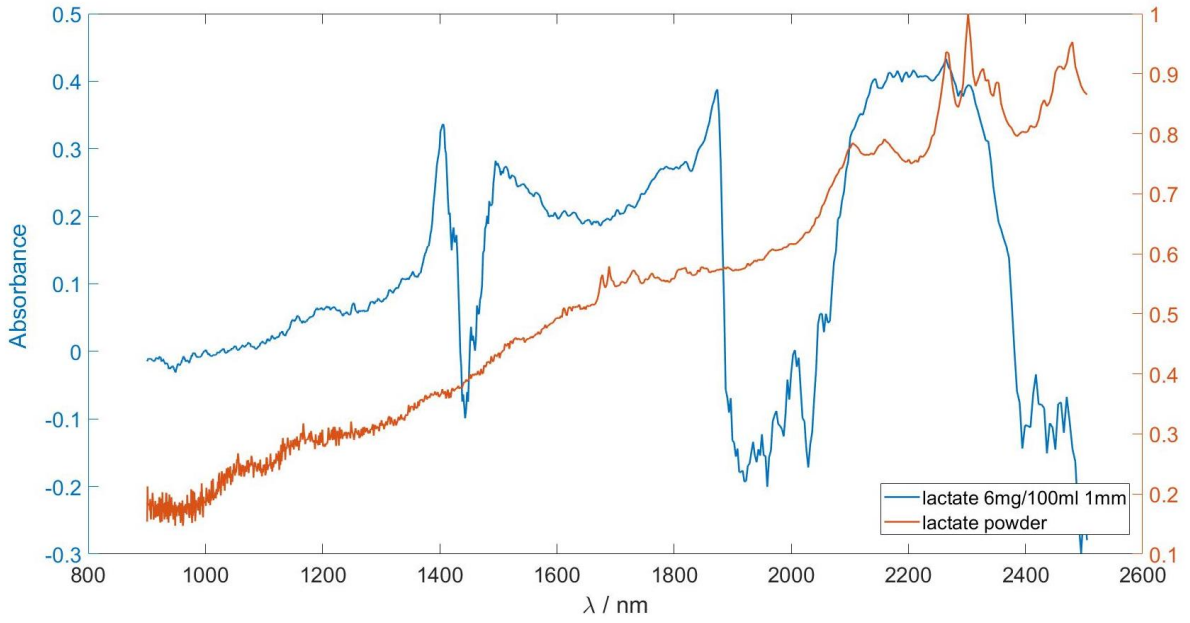

Figure 28 Sodium-L-lactate 6 mg/100 ml with the solution depth of 1 mm and sodium-L-lactate powder of twice absorbance

According to Lambert Beer's law the best absorbance spectrum was predicted at the distance of 0.3 mm. However, the best results were achieved with more solution at a gap of 1 mm. Furthermore, the same experiment was performed with the highest healthy blood lactate concentration of 20 mg/100 ml that correlates to 25 mg/100 ml of the sodium-L-lactate. The same phenomenon as previously perceived applies to this higher concentration. **Figure 29** illustrates also the three different quantities of solution 0 mm (blue graph), 0.3 mm (red graph) and 1 mm (yellow graph). Those three are compared to the absorbance spectra of the powder again. Both lactate peaks can be seen at 2247 and 2299 nm in the yellow graph.

Further, also the 1 mm absorbance spectrum was chosen to be compared to the spectrum of the lactate powder, due to the best distinct lactate peaks.

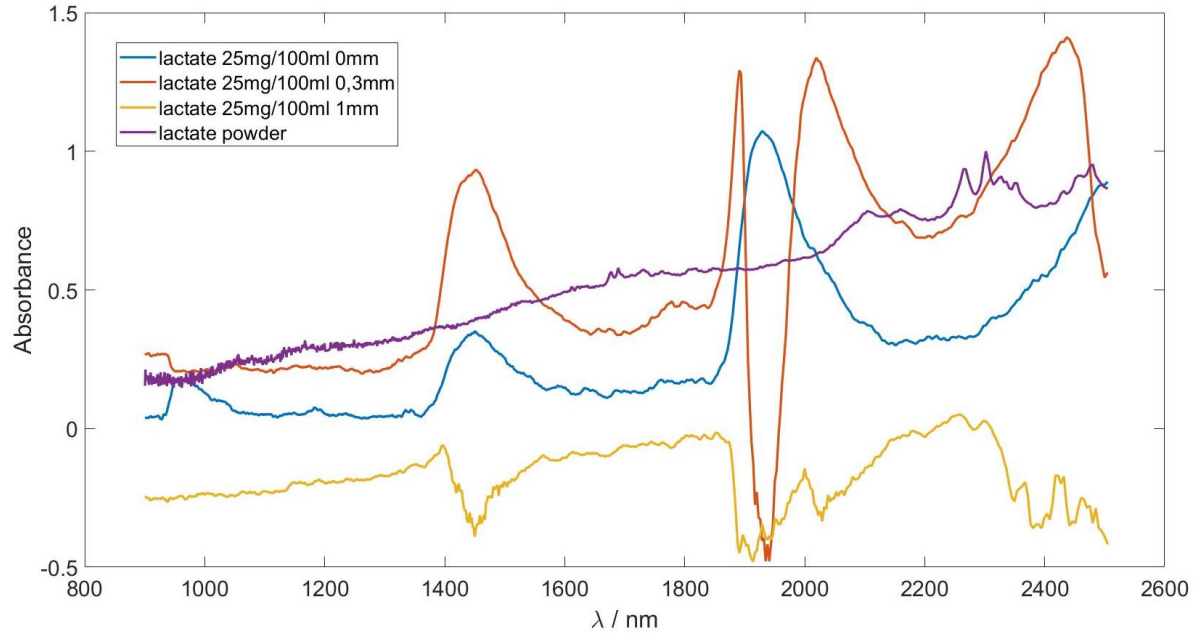

Figure 29 Absorbance of sodium-L-lactate 25 mg/100 ml with solution depths of 0 mm, 0.3 mm and 1mm and lactate powder

This results into superosing those two spectra and therefore identify, if the peaks fit each other. **Figure 30** pictures the absorbance of the sodium-L-lactate powder (red graph) and the absorbance spectrum of the 1 mm gap of 25 mg/100 ml sodium L-Lactate concentration.

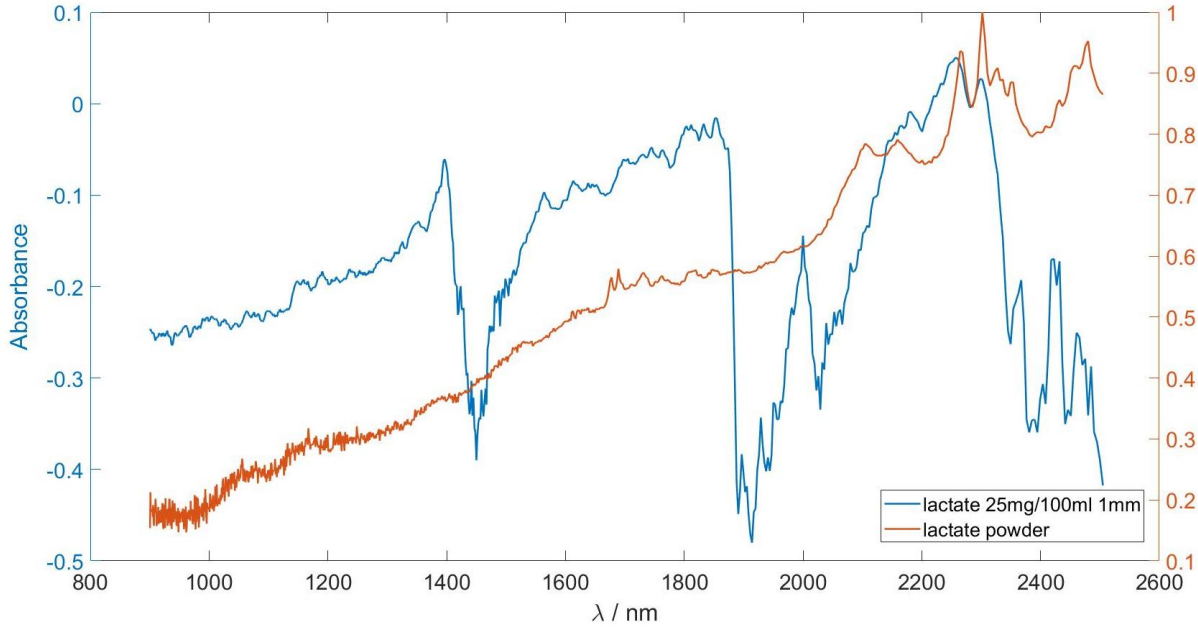

Figure 30 Sodium-L-lactate 25 mg/100 ml with the solution depth of 1 mm and sodium-L-lactate powder of twice absorbance

Finally, the same experiment was also carried out with the highest sodium-L-lactate concentration. This means 1.12 g/100 ml sodium-L-lactate got measured whereas 0.896 g/100 ml of lactate is present. Figure 31 shows again all three different volumes of sodium-L-lactate. Again, 0 mm (blue graph), 0.3 mm (red graph) and 1 mm (yellow graph) were compared to the pure sodium-L-lactate spectrum of the powder.

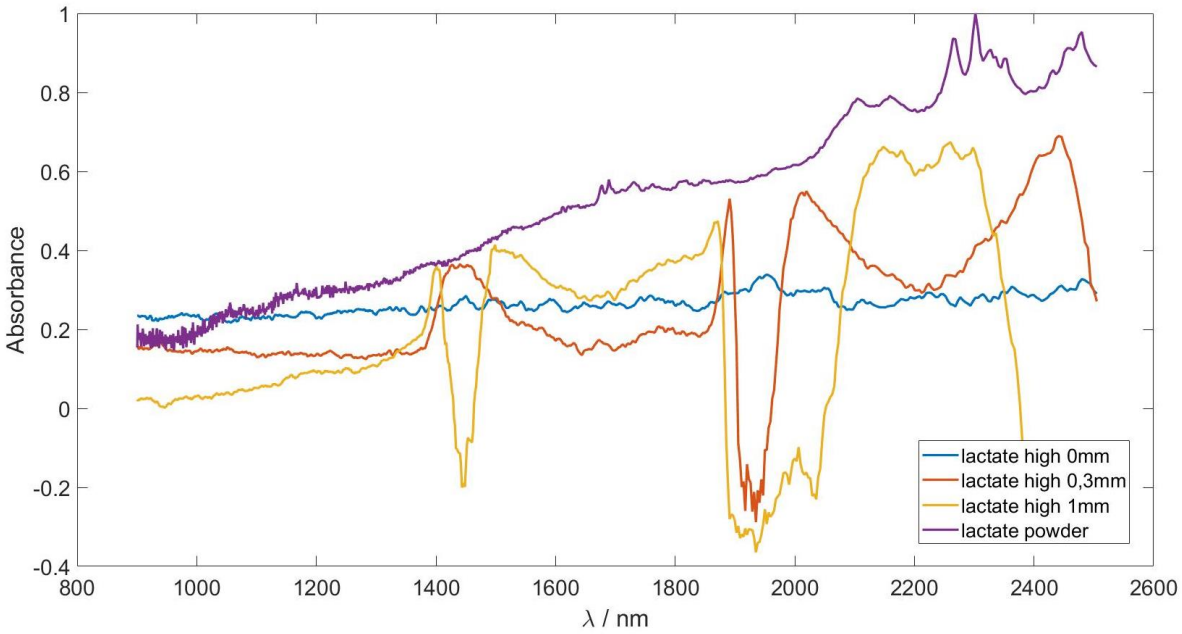

Figure 31 Absorbance of lactate 1.12 g/100 ml with solution depths of 0 mm, 0.3 mm and 1 mm and lactate powder

As previous, the 1 mm curve has the best fit that leads to a plot of those two curves as well. In the plot the blue graph is the spectrum of the sodium-L-lactate powder and the red graph is the 1.12 g/100 ml sodium-L-lactate solution. Once again, the two peaks fit each other perfectly.

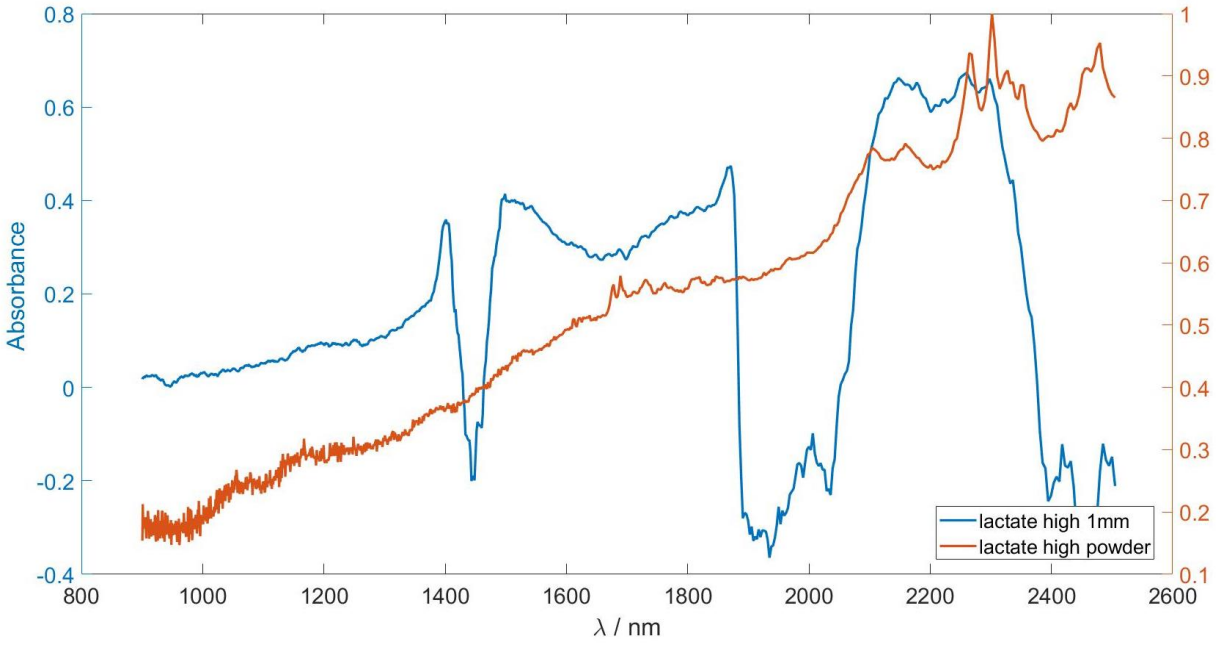

Figure 32 Sodium-L-lactate 1.12 g/100 ml with the solution depth of 1 mm and sodium-L-lactate powder of twice absorbance

The next step of the experiment was to try this measurement also on the other three biological molecules: urea, glucose and cholesterol. Compared to the sodium-L-lactate measurement, only one concentration of each molecule was tested. The setup is the same, it has been measured three different quantities of solution with the gaps of 0 mm, 0.3 mm and 1 mm. In the MATLAB plot underneath, **Figure 33** illustrates the absorbance spectra of urea with the concentration of 48 mg/100 ml. Again, we compare the three different thicknesses 0 mm (blue graph), 0.3 mm (red graph), 1 mm (yellow graph) that are filled with the solution to the pure urea powder spectrum (purple graph). As above, in the lactate measurement series the 1 mm approach fits the best.

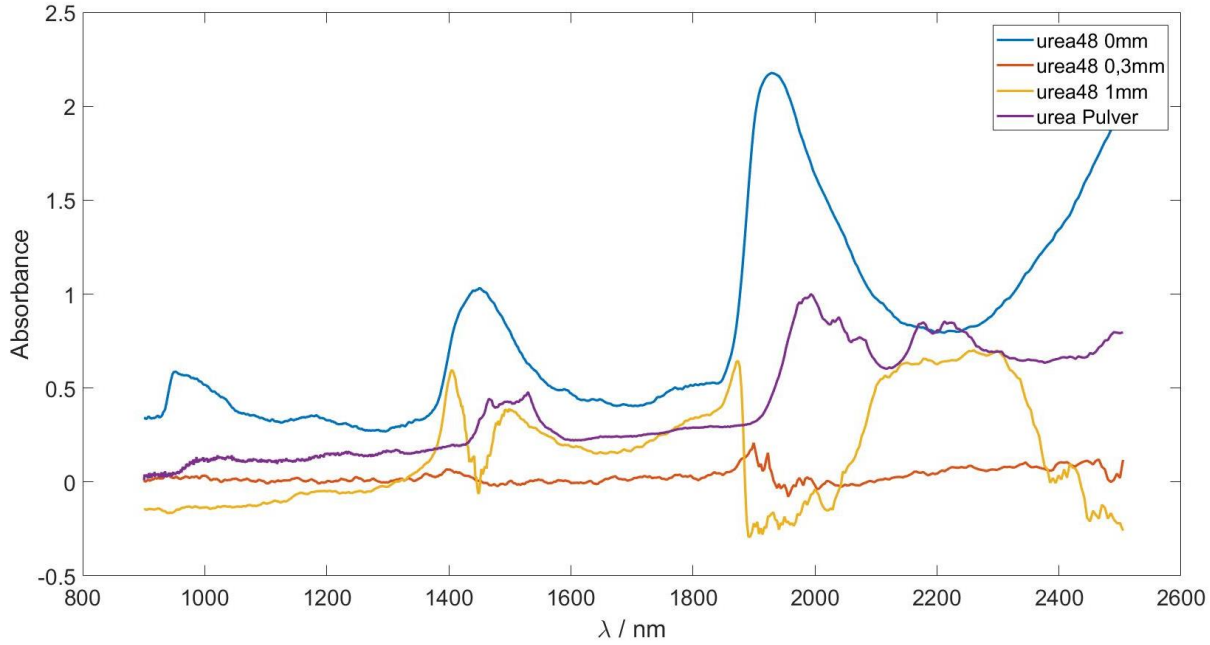

Figure 33 Urea 48 mg/100 ml with solution depths of 0 mm, 0.3 mm and 1mm and urea powder

Figure 34 pictures the 1 mm urea solution (blue graph) and the urea powder (red graph). Because of the different absorbance heights, it is rather difficult to compare those two absorbance spectra. Nevertheless it is distinguishable, that in the wavelength region between 2200 and 2400 nm the peaks overlap.

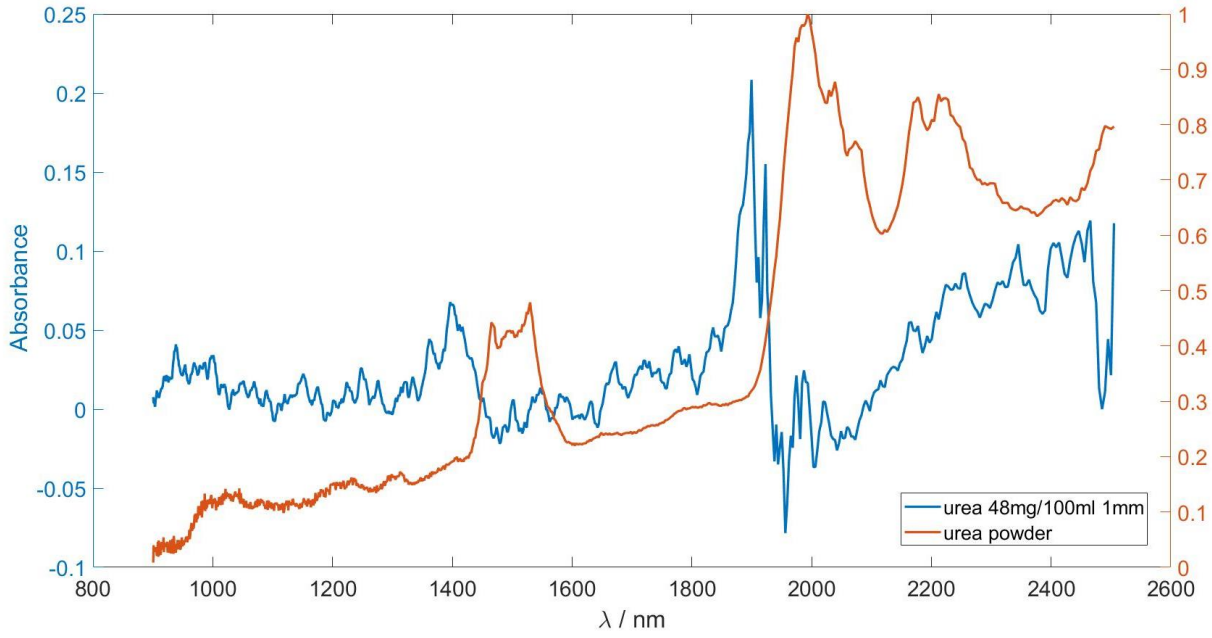

Figure 34 Urea 48mg/100ml with the solution depth of 1mm and urea powder of twice absorbance

Next, the biological molecule glucose was analysed. **Figure 35** shows the absorbance spectrum of the glucose powder, which does not have any extremely striking peaks. They are all weak. Consequently it is even more complex to measure those peaks of a small amount of glucose powder dissolved in distilled water. Therefore the results are as expected that in **Figure 36** are no peaks visible, no matter how thick the solution is: 0 mm (blue graph), 0.3 mm (red graph), 1 mm (yellow graph). Only in the yellow graph some weak signals can be observed.

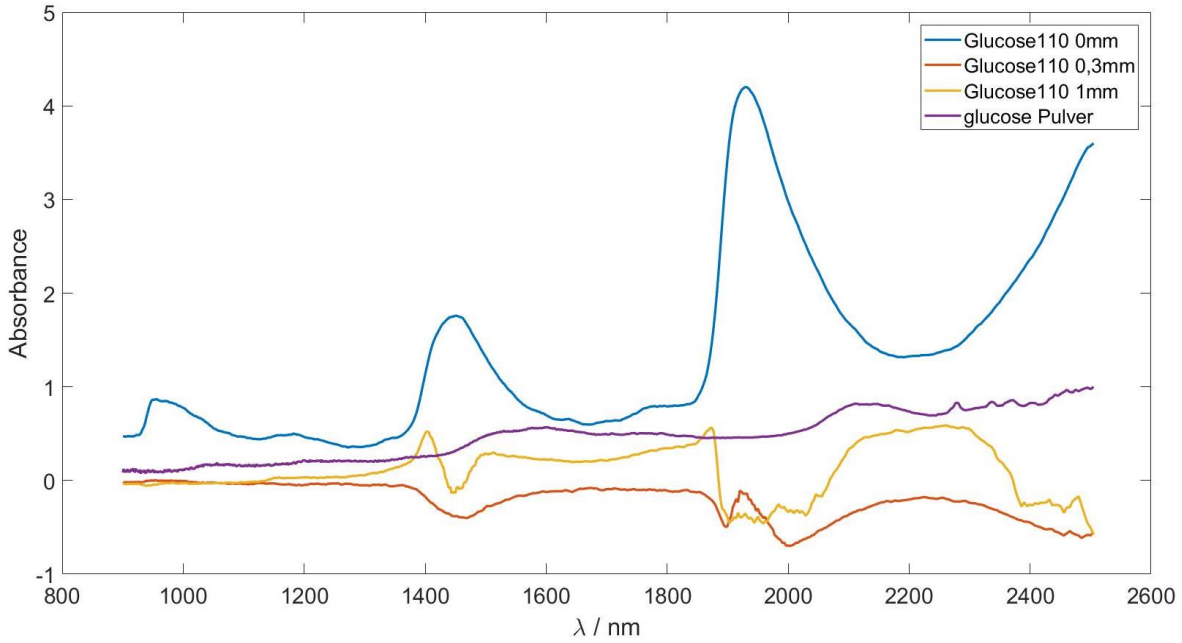

Figure 35 Glucose 110 mg/100 ml with solution depths of 0 mm, 0.3 mm and 1 mm and glucose powder

For this reason glucose 110 mg/100 ml was plotted with the 20 µl amount of the solution which equates the volume of the 1 mm gap. The highest peak of the glucose solution was detected at a wavelength of 2277 nm.

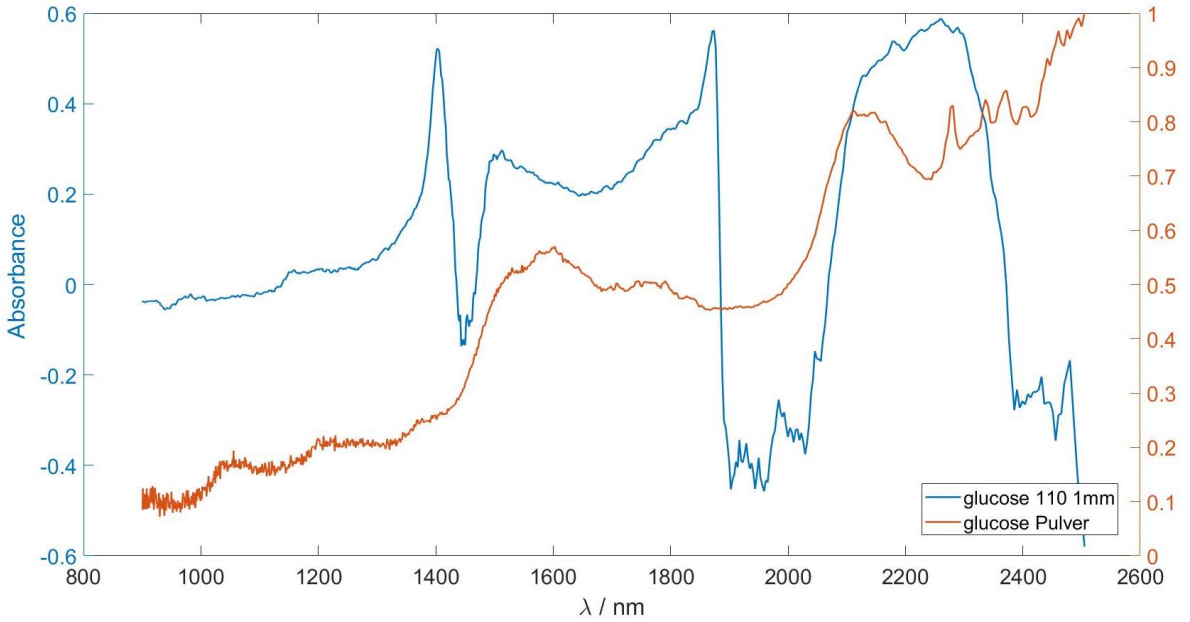

Figure 36 Glucose 110 mg/100 ml with the solution depth of 1mm and glucose powder of twice absorbance

Cholesterol is the last measurement in this spectrometry chapter. The problem with cholesterol is, that it is not soluble in water. That is why we do not have a homogenous solution, instead we have water with many cholesterol chunks. Further, this leads not to the aspired concentration of 200 mg/100 ml, instead it is much less. This explains why none of the three different solutions fits the cholesterol powder absorbance spectrum well.

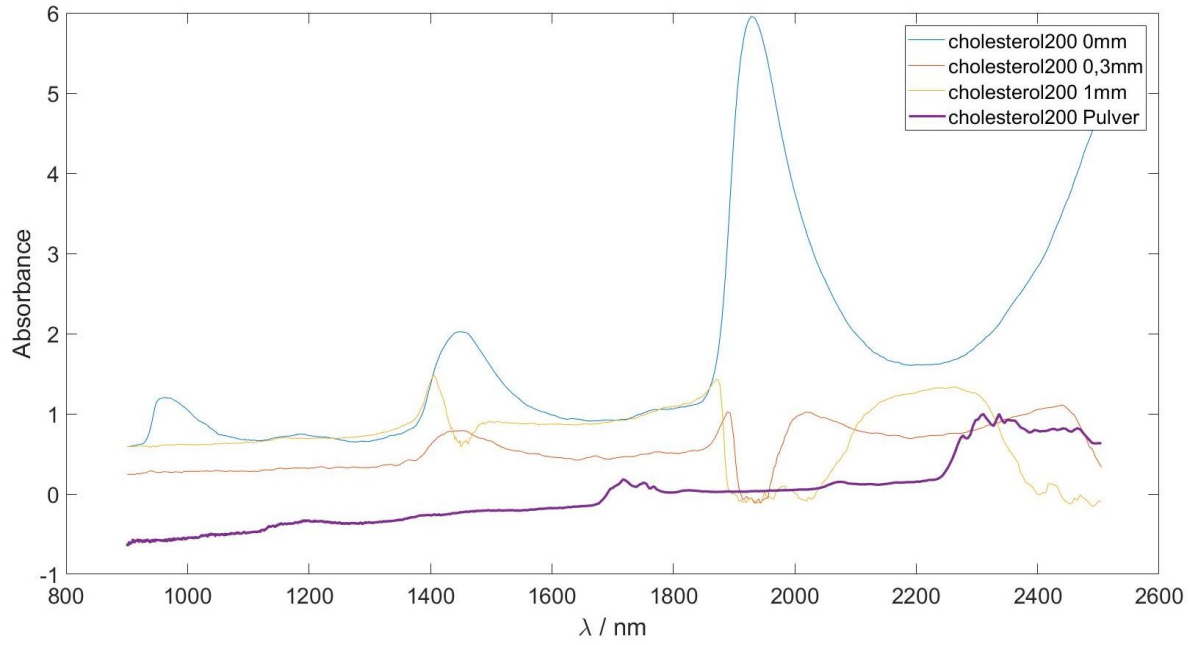

Figure 37 Cholesterol <<200 mg/100 ml with solution depths of 0 mm, 0.3 mm and 1 mm and cholesterol powder

To illustrate this better a MATLAB plot was performed. **Figure 38** shows the 1 mm gap, which is filled with cholesterol solution (blue graph), compared to the cholesterol powder absorbance spectrum (red graph). These two absorbance spectra do not match.

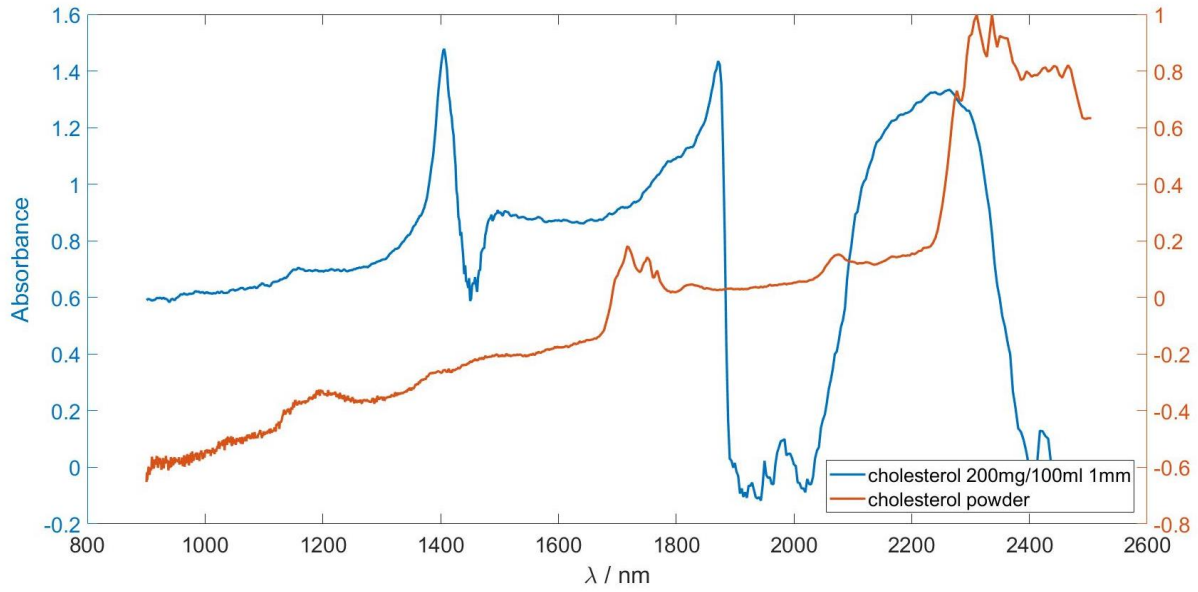

Figure 38 Cholesterol <<200mg/100ml with the solution depth of 1mm and cholesterol powder of twice absorbance

6.4 Discussion

The spectrometry is a good method to measure the sodium-L-lactate peaks precise within small concentrations. Nevertheless, water absorbs a lot of light, therefore it is not that easy and needs further improvements, like the spherical gold mirror to couple as much light as possible into the fibre, to measure the lactate. Another drawback is that it is an expensive method to determine the lactate peaks. Especially difficult is an adequate measurement of the other three biological molecules: urea, glucose and cholesterol. The problem was that the highest peaks of the powder and the solution are not at the same wavelength. Therefore, a comparison is tough. It was possible to measure the urea peaks, but the glucose peaks were nearly impossible to determine. The glucose peaks of the powder are nearly undetectable, with only small changes being observed. Therefore, it is even harder to measure those glucose peaks in low concentrations. Further, cholesterol is the hardest biological molecule to measure due to its low solubility in water. That leads to a concentration which is a lot smaller than the achieved 200 mg/100 ml. In summary, it is a good measuring method for sodium-L-lactate. It is possible to measure the peaks accurately. The higher the concentration in the solution is, the more distinct the peaks are. However, the result for cholesterol is not usable, due to the low solubility and therefore mostly solid residue being present.

7 Measurements with Photoacoustic Spectroscopy

7.1 History

The essential effect for photoacoustic spectroscopy (PAS) was already detected in 1880 by Alexander Graham Bell while experimenting on the transmission of sound via a beam of collimated sunlight. Bell replaced the detector of a conventional spectrograph with a hearing tube and created a photophone, which reflected a beam of the sunlight onto a selenium cell [35] [36]. The applicability of PAS was initially limited. As long as the sun was the most common light source and the human ear was the only detector available, no reliable quantitative analysis was possible [36]. The first PAS spectroscopy applications described in literature by Viegerov was in 1938. Viegerov used this technique for gas concentration measurement with a broadband infrared light source [35] [36]. In the middle of the seventies, the theoretical foundation of the optoacoustic effect was described with the Rosencwaig-Gersho theory (RG-theory) and therefore technically usable. Nevertheless, these systems were highly complicated, sophisticated and expensive. Only with the wide spread of relatively low-cost, compact lasers and further telecommunication-type diode lasers in the 90s, photoacoustic instruments become convenient for practical applications in environmental monitoring or industrial process control [35]. The high detection sensitivity of photoacoustic spectroscopy was only achieved through the invention of high-performance lasers, sensitive capacitor microphones and low noise amplifiers [37].

7.2 Theory

Photoacoustic Spectroscopy is used in many different applications. The big advantage of this technique is that it is a non-invasive method. Evidently, the focus in medicine is measuring as many medical tests non-invasive as possible. For the last decades, especially glucose concentration has been measured like this [1]. Photoacoustic Spectroscopy is a highly sensitive and selective measurement method, which is often used if you have marginal concentrations of one molecule in the presence of other gases or fluids [37]. PAS is notably

common for gas concentration measurement application, but there are also several studies where this effect is used for the measurement of biological molecules [1]. The PAS belongs to the optothermal techniques: It converts optical energy into thermal energy and is based on the photoacoustic effect. To conclude, the technique's basic principle is a modification of pressure, temperature or density that can be measured. Therefore, optothermal spectroscopy is an indirect measuring method [38]. Impinging monochromatic light upon a sample creates a localized short duration heating due to the absorption of light by the body fluids. As a result, the thermal expansion produces an ultrasonic pressure wave that can be detected by a suitable transducer, e.g. a microphone [1].

The big advantage of photoacoustic spectroscopy is the linear relation between concentration and the measured signal. In our case, it represents the lactate. Consequently, the higher the concentration in the solution, the higher is the photoacoustic signal. Formula (15) shows this correlation [35].

$$S = P \cdot M \cdot \left(C \cdot \sum_{i=1}^{n} \eta_i \cdot \alpha_i \cdot c_i + A_b \right) \tag{15}$$

Whereas,

S……. photoacoustic signal in mV

P…….exciting light power in W

M……. sensitivity of the microphone in mV/Pa

C……..cell constant in $Pa \cdot cm \cdot W^{-1}$

α_i……..molar optical absorption coefficient of the light absorbing components at the wavelength of the exciting light in $cm^{-1} \cdot mol^{-1} \cdot dm^3$

c_i……..concentration of the light absorbing components in mol/dm3

A_b…….background signal generation efficiency in Pa/W

7.2.1 Photoacoustic effect

For the comprehension of the photoacoustic spectroscopy it is necessary to understand the photoacoustic effect. This effect describes the acoustic wave generation by absorption of a beam of light in gaseous, fluid or solid samples. In chapter 6 an absorption spectrometry was performed to investigate lactate, urea, glucose and cholesterol with different concentrations. As a result of light absorption, the molecules are excited and can relax by three different mechanism.

The first relaxation process emits a photon and is also called fluorescence [35]. This mechanism is only pertinent to molecules in the UV and visible light region. Therefore, it is irrelevant for the lactate concentration measurement, as the relevant lactate peaks are located in the infrared region. Further, the second relaxation process is based on a collision with another molecule, which results in an energy conversion process: The absorbed photon energy is transduced into translational energy. This type of relaxation generates a PA signal. This conversion derives from localized short duration heating due to the absorption of monochromatic light. Additionally, this thermal expansion increases temperature and further increases the pressure as well. Because of the modulated irradiating light, these temperature and pressure variations are periodic and generate acoustic waves in the samples [35]. Lactate concentration measurement by PAS is based on detecting the produced sound signal. This can be done with suitable transducers. In our case, a microphone was utilized. Finally, the third relaxation process is also based on a collision with another molecule, which becomes excited. The originally excited molecule returns to ground state. This phenomena is also called an inelastic collision. In combination with the second scenario, it also leads to a PAS signal. However, mainly the second relaxation process is responsible for a generated PAS signal [35].

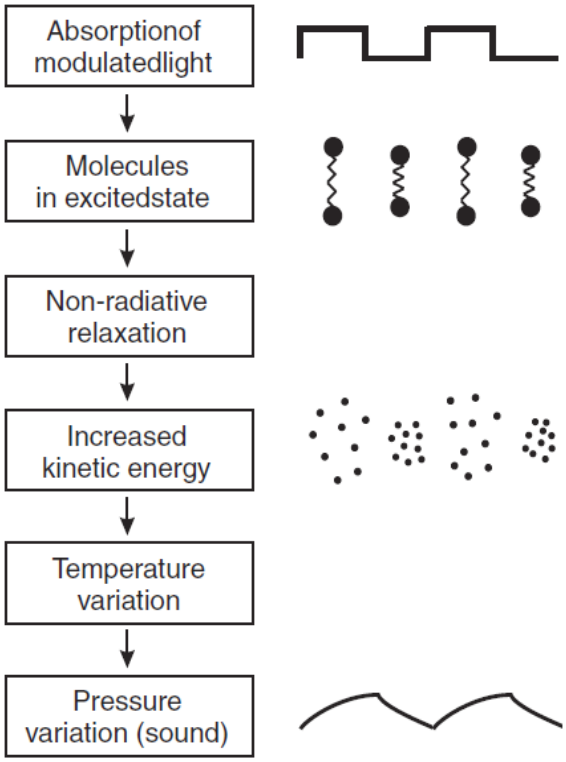

Figure 39 Process of photoacoustic signal generation [35]

7.2.2 Photoacoustic Lactate signal

In our experiment we used the photoacoustic spectroscopy in the near- infrared region (NIR) for non-invasive lactate measurement, which is also called near-infrared spectroscopy (NIRS). The NIR-spectroscopy uses the light in the 750-2500 nm region. As mentioned in the light chapter, the infrared radiation divides into IR-A, IR-B and IR-C. The strongest lactate peaks are located within the IR-B region. The NIRS approach is based on absorption spectroscopy. The penetration of infrared radiation in skin is much deeper than visible or middle-infrared radiation. The NIR spectral region possesses a few windows where haemoglobin, lipid and water signals are low enough to get a good reliable result for the lactate measurement [1]. A further important fact is that the penetration of light into skin decreases with the increase in wavelength [1]. The NIR-spectroscopy is frequently used for biological molecules, because of the high amount of carbon, nitrogen and hydrogen components in biological tissue. The NIR-range particularly measures the C-H, N-H and O.-H bands, in particular.

7.3 Methods

For the practical part of the experiment a printed circuit board (PCB) was designed in KiCad. First, a suitable microphone was chosen, which is able to detect the slight sound changes and can handle the liquid solution. The picked model is a microelectromechanical system (MEMS) microphone, which is very small; PMM-3738-VM1000-R from pui audio. It is also dust and water resistant according to IP57. To increase the output signal it is essential to amplify the output signal of the MEMS microphone. Therefore, an amplifying circuit with two inverting amplifiers was designed, whereas the first amplifier has a gain of 10 (A= -10) and the second one has a gain of 100 (A= -100). In total, the output of the microphone gets intensified with a positive factor of A = 1000. **Figure 40** illustrates the whole circuit layout. To stabilise the circuit, additional resistors and capacitors have been added: The capacitors and resistors are spread into 3 different areas. For instance, the red circle marks the resistors R7 and C8, which serve a current limiting purpose. On the other hand, the blue circles represent AC coupling capacitors. A relatively high capacitance (10 µF) guarantees only the passing of low frequencies. The last ones are the yellow circles, which are located in the feedback networks of the amplifiers and act as active low pass filters. With the resistor it is possible to limit the amplification of low frequencies. To conclude, with this arrangements it is possible to measure the minute photoacoustic signal, to amplify it and to improve the signal to noise ratio (SNR). It is important to protect the electronic components against over- and undervoltages. In that case, the protection circuit was realized by two voltage controllers, one for the positive (+ 3.3 V) region and one for the negative region (- 3.3 V).

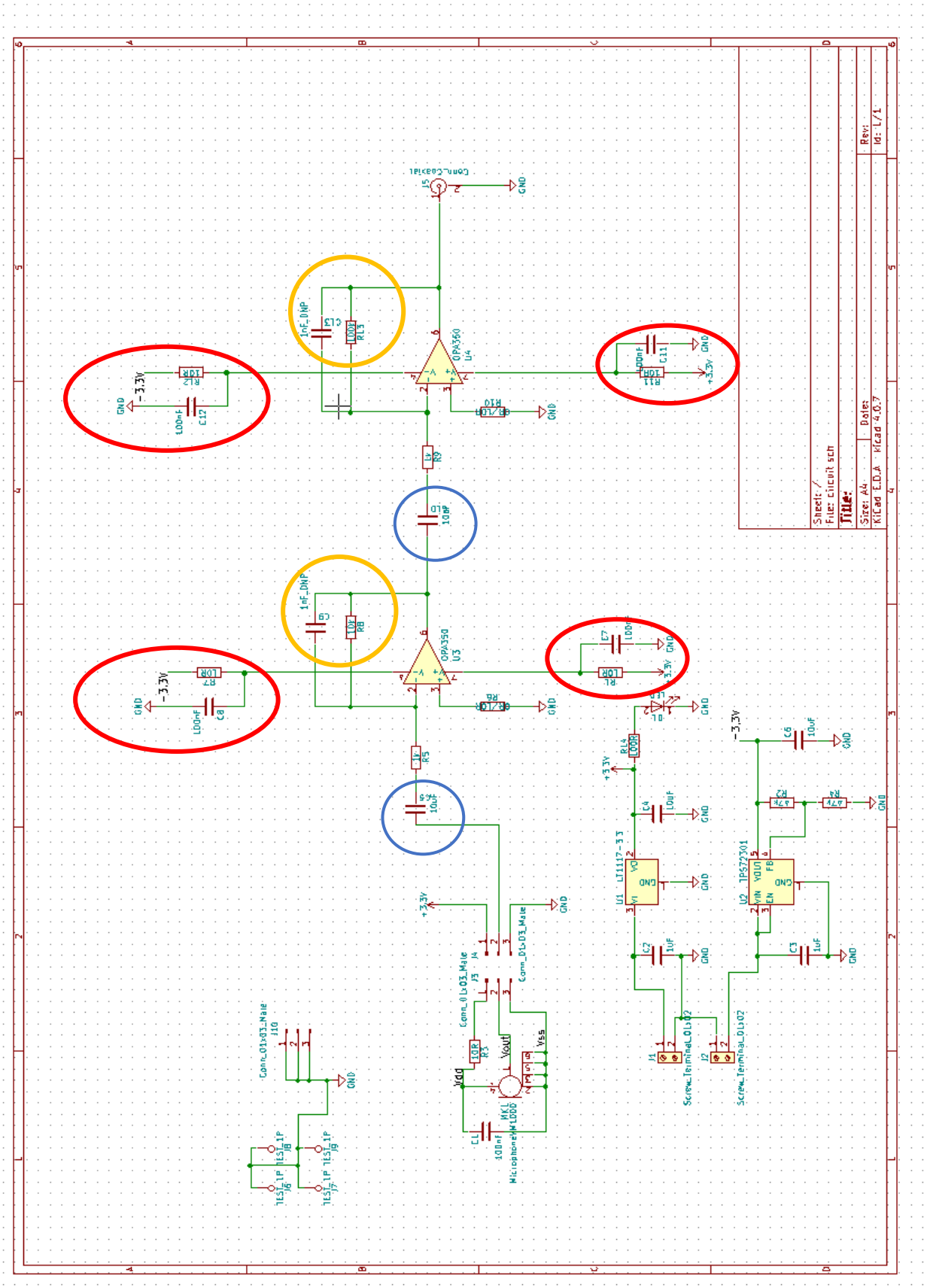

Figure 40 Circuit layout for the photoacoustic spectroscopy measurement

In **Figure 41** the final result of the printed circuit board is illustrated. As pictured, the PCB is separated into two parts. The small PCB contains the MEMS microphone, a resistor and a capacitor. This size has been chosen to fit exactly on the cuvette, which contains the solution of sodium-L-lactate in distilled water. Therefore, the PCB acts as a cap of the cuvette to allow pulling over for further observation and to immerse the microphone totally in the solution.

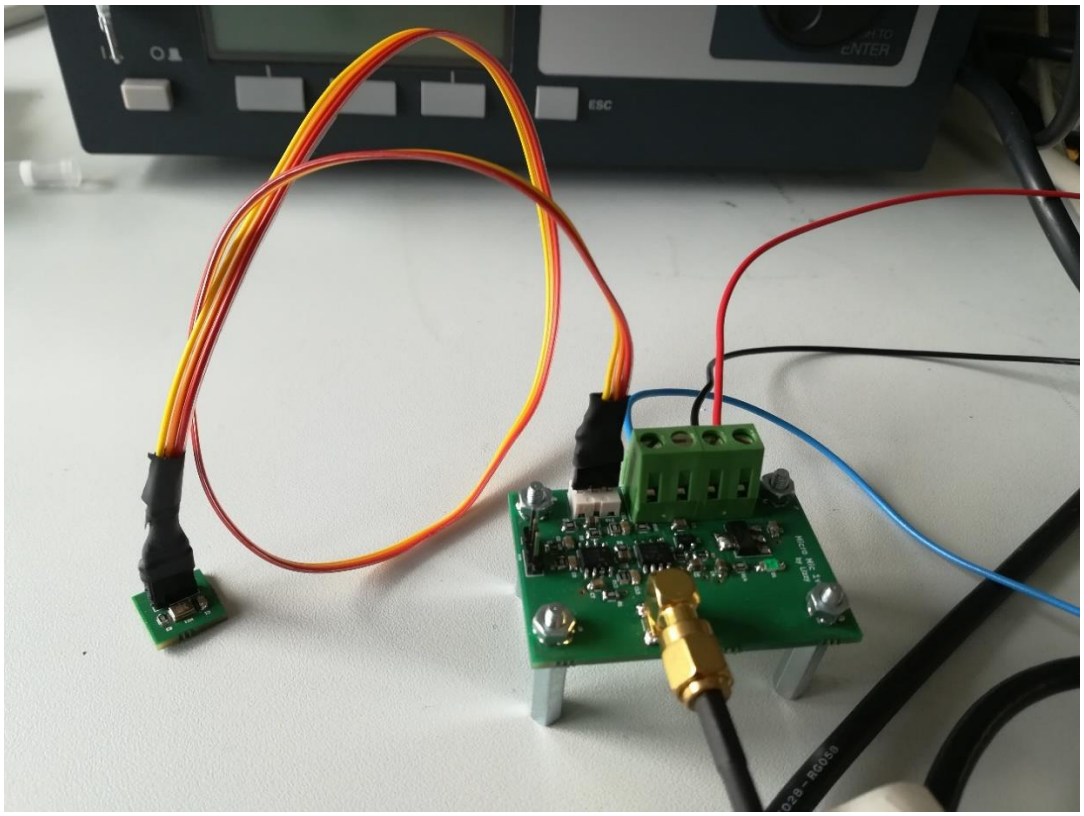

Figure 41 PCB of the microphone and the second PCB for amplification

To guarantee the same conditions for each measurement (repeatability and reproducibility), the setup needed a special 3D-printing: To avoid leaking of the solution, the cuvette and the small PCB were fixed with elastic bands. **Figure 42** depicts the above described setup.

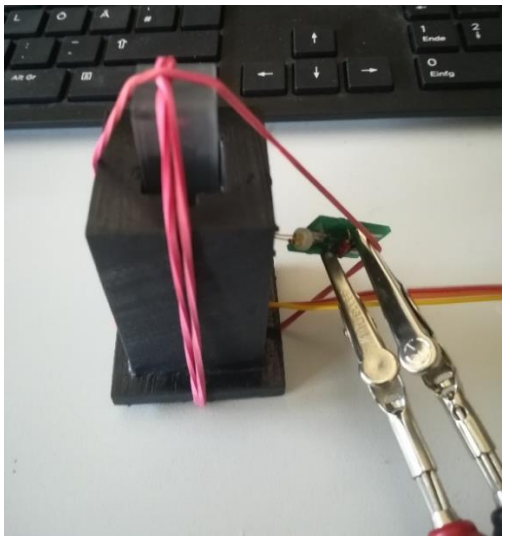

Figure 42 3D-printing as a holder for the cuvette and the small PCB in between

Another essential part of this experiment is getting a pulsed signal. Only with pulses a photoacoustic signal is even possible. To obtain a pulsed signal, a special LED in the infrared region and a laser diode driver for triggering were needed. The LED is called LED2350P and has an optical power pulse mode at 1 Ampere with P = 16 mW. Although, some complications occurred with the laser driver, it was externally triggered by a waveform generator. In addition, the name of the laser diode driver is ITC4001 Laser Diode/Temperature Controller and manufactured by Thorlabs. The frequency of the waveform generator was set at 2 kHz but the current could not reach 1 A, it was only possible to achieve 500 mA and as a result, the total power is less than the 16 mW.

To measure very small signals it is essential to use a lock-in amplifier. This device minimizes disturbing noise influence and its use is quite common in photoacoustic spectroscopy. Usually, it is an electronic device, which is nowadays often implemented digitally. It only detects the signal part of the modulation frequency [38]. Therefore, it allows the extraction of infinitesimal signals with a known frequency from a much higher noise background. The signal to noise ratio (SNR) can be as small as -50 dB [36].

The lock-in amplifier splits the signal input into an in-phase part (I) and a quadrature part (Q) and reveals the phase shift between the external reference frequency and the detected signal [38]. Within this experiment, a digital lock-in amplifier was used.

7.4 Results

The first step was verifying the function of the designed circuit with the oscilloscope. At this part of the experiment there was no lock-in amplifier attached. The test was performed with each sodium-L-lactate concentration (6 mg/100 ml, 25 mg/100 ml and 1.12 g/100 ml) in distilled water. The results are satisfying: After an impulse the lactate in the solution gets excited, which leads to a photoacoustic signal that can be recorded with the microphone. In **Figure 43** the acoustic signal is clearly visible. The yellow line represents the pulse, the purple line the microphone output (the photoacoustic signal) and the blue line the wave generator output. Accordingly, an oscillation of the output signal - directly after the pulse excites the lactate in the solution - is detectable.

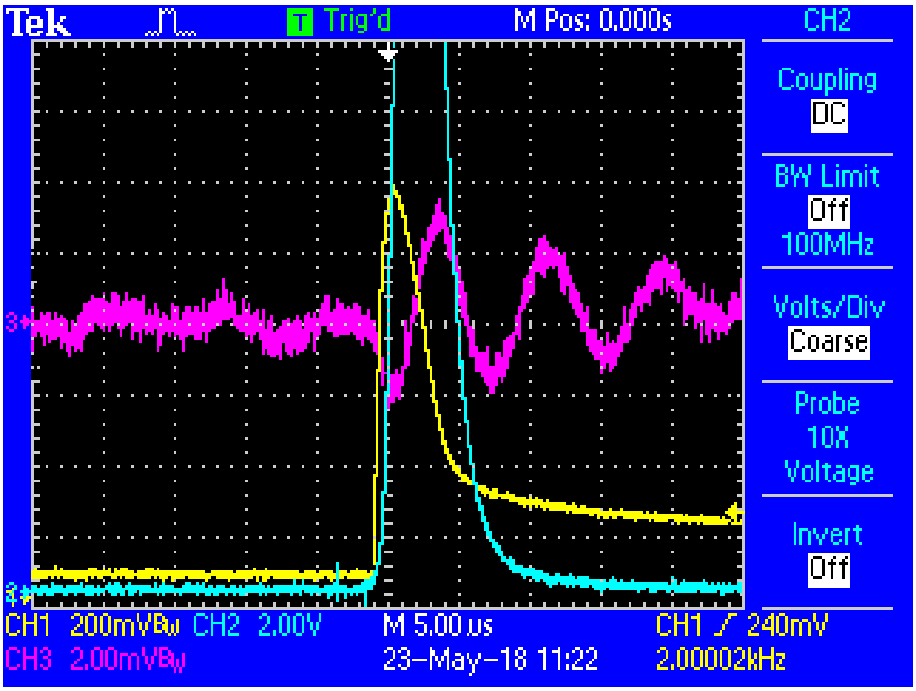

Figure 43 Oscilloscope picture of the photoacoustic signal: The yellow graph represents the pulse, the purple graph the photoacoustic signal and the blue graph the wave generator output

The final step is to run the whole photoacoustic measurement including the Lock-in amplifier which allows an exact determination of the signal over the time. The signal was recorded over a period of 2 min, afterwards, the mean value of the whole recorded signal was taken to get rid of any outliers. This procedure was performed with each lactate solution and with distilled water. In sum, four signals have been recorded and each got averaged in the end. In

addition, the distilled water was set as a baseline and was subtracted from the three different sodium-L-lactate and distilled water solutions. Last, a MATLAB plot, which takes into account the lock-in amplified signal in relation to the lactate concentration, was generated, see **Figure 44**:

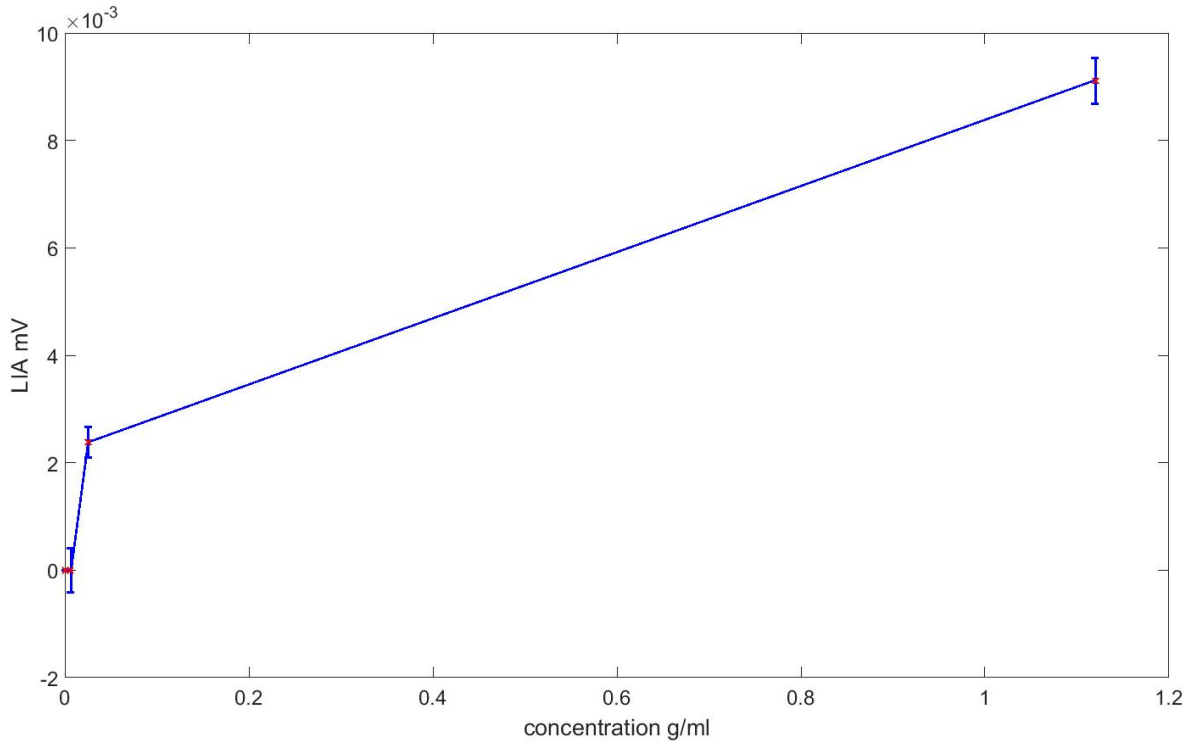

Figure 44 Dependence of the Lock-in amplified photoacoustic signal on the concentration

7.5 Discussion

In summary it is possible to measure the sodium-L-lactate in minute concentrations as they may occur in the human body. The higher the concentration of the sodium-L-lactate gets, the higher is the lock-in amplified signal. Ideally the results in **Figure 44** should be linear. The concentrations used, especially the really high one of 1.12 g/100 ml compared to the other two 6 mg/100 ml and 25 mg/100 ml distorts the result. That is why this measurement series should be redone with more concentrations to prove the linearity of the lock-in amplified signal.

8 Outlook and Limitations

The feasibility study should be the base of a future lactate sensor. In this thesis three different approaches were investigated: simulations with bandpass and Etalon and the two measurements, spectrometry and photoacoustic spectroscopy. The Etalon simulation showed that it should be possible to detect the lactate peaks in presence of other molecules and therefore to determine the lactate signal strength. The bandpass simulation was not able to solely detect the lactate peaks because of a not suitable (too wide) filter bandwidth. Within the spectrometry measurement expected results were obtained, although outliers were produced easily and ten measurements of each solution had to be performed. Within the photoacoustic measurement some problems occurred. This experiment should be redone with more concentrations and a current of 1 A, so that the power of 16 mW can be reached. With this adaptation it should be possible to get a linear Lock-in amplified signal and therefore a cheaper measuring method compared to the spectrometry measurement.

A limitation of creating in the future a lactate sensor would be that fat has a peak at exact the same wavelength of 2299 nm (**Figure 45**). Therefore, only low fat parts of the body can be analysed, for example, the finger or the earlobe.

Glucose[a]	Water[b]	Hemoglobin[b]	Fat[b]	Protein[b]
714	749			
		760 (E)		
			770	
		805 (E)		
		820 (E)		
	880			
939		910	920	910
	980			
1126	1211	1020 (E)	1040	1020
1408	1450			
1536				
1688				
	1787			
	1934			
2261			2299[c]	2174[d]
2326			2342[c]	2288[d]

[a] Calculated from glucose fundamental vibrations.
[b] "E" indicates an electronic absorption band; others are vibration overtone and combination bands *(19, 31)*.
[c] From Burmeister et al. *(14)*.
[d] From Pan et al. *(38)*.

Figure 45 Near-IR bands for components of solid tissue demonstrating potential interferences with NI lactate detection [39]

These areas are not commonly used for medical tests, as they are not as convenient as for example the wrist for heart rate watches. Further, the weak photoacoustic lactate signal, is difficult to measure accurately in the presence of water. To summarize it is possible to create a lactate sensor based on this research, but there are limiting factors, making accurate measurements in the blood very difficult.

9 List of References

[1] J. Yadav, A. Rani, V. Singh and B. M. Murari, "Prospects and limitations of non-invasive blood glucose monitoring using near-infrared spectroscopy," *Elsevier,* 2015.

[2] I. Ibraheem, *Medical Laser Technology VO,* Graz, 2016.

[3] B. Meffert and H. Meffert, "Optische Strahlung und ihre Wirkung auf die Haut," *Biomed. Technik,* 2000.

[4] Adolf Thies GmbH & Co. KG, "Thies Clima," [Online]. Available: https://www.thiesclima.com/de/Strahlung/. [Accessed 31 July 2018].

[5] D. Barolet, F. Christiaens and M. R. Hamblin, "Infrared and Skin: Friend or Foe," *J Photochem Photobil B.,* February 2016.

[6] B. H. Mahmoud, C. L. Hexsel, I. H. Hamzavi and H. W. Lim, "Effects of Visible Light on the Skin," *Photochemistry and Photobiology,* 2008.

[7] P. Schieke, P. Schröder and J. Krutmann, "Cutaneous effects of infrared radiation: from clinical observations to molecular response mechanism," *Photodermatology, Photoimmunology & Photomedicine,* 2003.

[8] T. Höll and G. Holler, *Optische Methoden in der Messtechnik, Labor,* Graz, 2015/16 WS.

[9] K. J. Gunnerson, "Medscape: "Lactic Acidosis"," emedicine.medscape, 6 march 2017. [Online]. Available: https://emedicine.medscape.com/article/167027-overview. [Accessed 31 july 2018].

[10] "Wikipedia: "Lactate"," [Online]. Available: https://de.wikipedia.org/wiki/Lactate. [Accessed 1 july 2018].

[11] M. Savigny and J. Berzon, "VetFolio," January 2006. [Online]. Available: http://www.vetfolio.com/clinical-pathology/measuring-blood-lactate-levels. [Accessed 15 May 2018].

[12] M. L. Goodwin, J. E. Harris, A. Hernandez and B. Gladden, "Blood Lactate Measurements and Analysis during Exercise: A Guide forl Clinicians," *Journal of Diabetes Science and Technology,* 4 July 2007.

[13] W. Patrick, W. Bloch and J. Mester, "Moderne Betrachtundsweisen des Laktats: Laktat ein überschätztes und zugleich unterschätztes Molekül," *Sportmedizin und Sporttraumatologie,* 2009.

[14] C. Higgins, "Acuratecaretesting," October 2007. [Online]. Available: https://acutecaretesting.org/en/articles/lactate-and-lactic-acidosis. [Accessed 8 May 2018].

[15] M. Ren and M. A. Arnold, “Comparison of multivariate calibration models for glucose, urea, and lactate from near-infrared and Raman spectra,” *Analytical and Bioanalytical Chemistry,* 3 January 2007.

[16] P. Li, “LinkedIn: "What is Triacetin",” March 2016. [Online]. Available: https://www.linkedin.com/pulse/what-triacetinglycerol-triacetate-bruce-zhao. [Accessed 8 May 2018].

[17] K. H. Hazen, M. A. Arnold and G. W. Small, “Measurement of glucose and other analytes in undiluted human serum with near-infrared transmission spectroscopy,” *Elsevier,* 28 April 1998.

[18] “Wikipedia: "Urea",” 19 July 2018. [Online]. Available: https://en.wikipedia.org/wiki/Urea. [Accessed 31 July 2018].

[19] “Medicinenet,” 13 May 2016. [Online]. Available: https://www.medicinenet.com/script/main/art.asp?articlekey=5905. [Accessed 31 July 2018].

[20] “Encyclopaedia Britannica: "Glucose",” 19 April 2018. [Online]. Available: https://www.britannica.com/science/glucose. [Accessed 31 July 2018].

[21] “Britannica: "Cholesterol",” Encyclopaedia Britannica, 12 July 2018. [Online]. Available: https://www.britannica.com/science/cholesterol. [Accessed 31 July 2018].

[22] V. Saptari and K. Youcef-Toumi, “Design of a machanical-tunable filter spectrometer for noninvasive glucose measurement,” *Applied Optics,* 1 May 2004.

[23] “Edmund Optics: "Optial Filters",” Edmund Optics, [Online]. Available: https://www.edmundoptics.de/c/optical-filters/610/. [Accessed 31 July 2018].

[24] “Spektrum: "Fabry-Perot-Interferometer",” Spektrum, [Online]. Available: https://www.spektrum.de/lexikon/physik/fabry-perot-interferometer/4685. [Accessed 31 July 2018].

[25] A. Hauser, *Experimental methods of spectrosccopy, quantum optics & quantum measuring techniques "VO Unterlagen",* Graz, 2016.

[26] S. Giglberger, “Uni Regensburg: "Versuch „fp“: Fabry-Perot-Interferometer",” Uni Regensburg, 2010. [Online]. Available: http://www.physik.uni-regensburg.de/studium/praktika/b/download/fabry.perot.pdf. [Accessed 31 July 2018].

[27] “Wikipedia: "Fabry-Perot interferometer",” Wikipedia, 5 July 2018. [Online]. Available: https://en.wikipedia.org/wiki/Fabry%E2%80%93P%C3%A9rot_interferometer. [Accessed 31 July 2018].

[28] “Dictionary: "Reflactance",” Dictionary, 2016. [Online]. Available: https://www.dictionary.com/browse/reflectance.

[29] Layertec Optical Coatings, *Angebot Etalon,* Mellingen, 2018.

[30] Arcoptix Switzerland, Installation and Operation Manual Arcospectro FT Rocket Fourier-Transform Spectroscopy Software Version 2.1, 2015.

[31] "Wikipedia: "Absorption (Physik)"," 20 June 2018. [Online]. Available: https://de.wikipedia.org/wiki/Absorption_(Physik). [Accessed 31 July 2018].

[32] B. Flournoy, "Sciencing: "Difference between optical density and absorbance"," 4 June 2018. [Online]. Available: https://sciencing.com/difference-between-optical-density-absorbance-7842652.html. [Accessed 31 July 2018].

[33] "Wikipedia: "Absorbance"," Wikipedia, 22 April 2018. [Online]. Available: https://en.wikipedia.org/wiki/Absorbance. [Accessed 31 July 2018].

[34] "Wikipedia: "Lambert-Beersch'es Gesetz"," Wikipedia, 27 July 2018. [Online]. Available: https://de.wikipedia.org/wiki/Lambert-Beer%E2%80%99sches_Gesetz. [Accessed 31 July 2018].

[35] Z. Bozoki, A. Pogany and G. Szabo, "Photoacoustic Instruments for Practical Applications: Present, Potentials and Future Challenges," *Applied Spectroscopy,* 2011.

[36] C. Haisch, "Photoacoustic spectroscopy for analytical measurements," *Measurement Science and Technology,* 25 November 2011.

[37] W. Demtröder, Laserspektroskopie, Berlin: Springer, 1991.

[38] P. Breitegger and C. Maier, *Sensorsysteme Labor: Spektroskopie und Photoakusik LU,* Graz, 2018.

[39] O. S. Khalil, "Spectroscopic and Clinical Aspects of Noninvasive Glucose Measurements," *Clinical Chemistry,* 1999.

10 Appendix

All crucial code sequences are shown in this chapter.

10.1 Simulation

10.1.1 Bandpass

```
Daten_2250=dlmread('BP2250-500.csv',';',1,0);
wavelength_2250=Daten_2250(1:end,1);
transmission_2250=Daten_2250(1:end,2);
transmission_2250=transmission_2250(wavelength_2250>=1900 &
wavelength_2250<=2900)/100;
%conversion into percentage (division by 100)

Daten_2500=dlmread('BP2500-500.csv',';');
wavelength_2500=Daten_2500(1:end,1);
transmission_2500=Daten_2500(1:end,2);
transmission_2500=transmission_2500(wavelength_2500>=1900 &
wavelength_2500<=2900)/100;
wavelength_plot = wavelength_2250(wavelength_2250>=1900 &
wavelength_2250<=2900);
bandpass_multiplication = transmission_2250.*transmission_2500;

%interpol bandpass_multiplication to wavelength_laktat
bandpass_multiplication_laktat = interp1(wavelength_plot,
bandpass_multiplication, wavelength_laktat, 'spline');
%limiting real_laktat from 1900 to 2900 nm
real_laktat=real_laktat(wavelength_laktat>=1900 & wavelength_laktat<=2900);
bandpass_multiplication_laktat=bandpass_multiplication_laktat(wavelength_la
ktat>=1900 & wavelength_laktat<=2900);
bandpass_laktat=real_laktat.*bandpass_multiplication_laktat;
wavelength_1900_2900 = wavelength_laktat(wavelength_laktat>=1900 &
wavelength_laktat<=2900);

real_gesamt=real_gesamt(wavelength_laktat>=1900 & wavelength_laktat<=2900);
bandpass_multiplication_gesamt = interp1(wavelength_plot,
bandpass_multiplication, wavelength_laktat, 'spline');
bandpass_multiplication_gesamt=bandpass_multiplication_gesamt(wavelength_la
ktat>=1900 & wavelength_laktat<=2900);
bandpass_gesamt=real_gesamt.*bandpass_multiplication_gesamt;
```

10.1.2 Etalon

```
%Etalon with calculated values:
lambda1=2299*10^-9;
lambda2=2247*10^-9;
n1=1.4334;
n2=1.4342;
lambda1_FS = 1603.88;    %lambda 1 in fused silica
lambda2_FS = 1566.73;    %Lambda 2 in fused silica
k = lambda2_FS/(lambda1_FS-lambda2_FS);
x = 6;
k=k*x;
L1=k*lambda1/(n1*2);
L2=(k+x)*lambda2/(n2*2);
L1=L2;
L=L1;
```

```
lambda_0 = 2299*1e-9;
delta_lambda = 52e-9;
n_refractindex = 1.4334;

% wavelength region
lambda = (2050:.1:2350).*1e-9;

% values for the model
theta = 0;  %irradiates directly on the probe (0° / 360°)
R_reflactance = 0.4202;  % Reflactance for fused silica at the wavelength
2299nm
l_length = L;

T_etalon_plot = @(lambda)
T_Etalon(lambda,R_reflactance,n_refractindex,l_length,theta);

function [ T_e ] = T_Etalon( lambda,R,n,l,theta )
%T_ETALON function based on equation
    delta = (2*pi./lambda)*2*n*l*cos(theta);
    T_e = (1-R).^2./(1-2*R*cos(delta)+R^2);
End
```

10.2 Measurements with Spectrometry

```
%import the 10 different measurements and summarize them
lactat25_1mm_i=zeros(10,890);
lactat25_1mm_window=zeros(10,890);
for k= 1:anzahl
    lactat25_1mm=dlmread(['lactat25 1mm 'num2str(k)'.csv'],';',1,0);
    lactat25_1mm_i(k,:)=lactat25_1mm(1:end,2);
lactat25_1mm_window(k,:)=conv(lactat25_1mm_i(k,:),ones(window,1)./
window,'same');
end
lactat25_1mm_calculated=sum(lactat25_1mm_window)/10;

%calculating the transmission and the absorbance
trans_lactat25_1mm=lactat25_1mm_calculated./water_1mm_calculated;
abs_lactat25_1mm=10*log10(1.0./trans_lactat25_1mm);
```

10.3 Measurements with Photoacoustic Spectroscopy

```
amplitude_mean=[mean(amplitude_laktat6) mean(amplitude_laktat25)
mean(amplitude_laktat_high)];

%calculating the LIA
vector_mean=zeros(3,1);
vector_mean(1,1)=mean_in_phase_laktat6;
vector_mean(2,1)=mean_in_phase_laktat25;
vector_mean(3,1)=mean_in_phase_laktat_high;

concentration=[0 0.006 0.025 1.12];

LIA6=sqrt((mean_in_phase_laktat6^2-
mean_in_phase_water^2)+mean_quadratur_laktat6^2-mean_quadratur_water^2);
LIA25=sqrt((mean_in_phase_laktat25^2-
mean_in_phase_water^2)+mean_quadratur_laktat25^2-mean_quadratur_water^2);
LIA_high=sqrt((mean_in_phase_laktat_high^2-
mean_in_phase_water^2)+mean_quadratur_laktat_high^2-
mean_quadratur_water^2);
```

```
LIA=[0 LIA6 LIA25 LIA_high];

%calculating the error bar
err1=std(laktat6_amplitude)-std(water_amplitude);
err2=std(laktat25_amplitude)-std(water_amplitude);
err3=std(laktat_high_amplitude)-std(water_amplitude);
error=[0 err1 err2 err3];
```